Chinese Journal of Natural Medicines

Naturally occurring *seco*– and *nor*–polycyclic polyprenylated acylphloroglucinols: distribution, structural diversity, andbiological activity

Yulin Duan, Ying Tang, Changxing Qi, Yonghui Zhang

Citation: Yulin Duan, Ying Tang, Changxing Qi, Yonghui Zhang, Naturally occurring *seco*– and *nor*–polycyclic polyprenylated acylphloroglucinols: distribution, structural diversity, andbiological activity, Chinese Journal of Natural Medicines, 2025, 23(7), 824–837. doi: 10.1016/S1875–5364(25)60911–3.

View online: https://doi.org/10.1016/S1875–5364(25)60911–3

Chinese Journal of Natural Medicines 23 (2025) 824-837

Contents lists available at ScienceDirect

Chinese Journal of Natural Medicines

journal homepage: www.cjnmcpu.com/

Review

Naturally occurring *seco*- and *nor*-polycyclic polyprenylated acylphloroglucinols: distribution, structural diversity, and biological activity

Yulin Duan[a,b], Ying Tang[d,*], Changxing Qi[c,*], Yonghui Zhang[c,*]

[a] *Department of Pharmacy, Traditional Chinese and Western Medicine Hospital of Wuhan, Tongji Medical College, Huazhong University of Science and Technology, Wuhan 430030, China*

[b] *Department of Pharmacy, Wuhan No. 1 Hospital, Wuhan 430022, China*

[c] *Hubei Key Laboratory of Natural Medicinal Chemistry and Resource Evaluation, School of Pharmacy, Tongji Medical College, Huazhong University of Science and Technology, Wuhan 430030, China*

[d] *Department of Pharmacy, Tongji Hospital, Tongji Medical College, Huazhong University of Science and Technology, Wuhan 430033, China*

ARTICLE INFO

Article history:
Received 9 April 2024
Revised 15 June 2024
Accepted 17 July 2024
Available online 20 July 2025

Keywords:
Natural products
Seco-polycyclic polyprenylated acylphloroglucinols
Nor-polycyclic polyprenylated acylphloroglucinols
Chemical structure
Biological activity

ABSTRACT

Polycyclic polyprenylated acylphloroglucinols (PPAPs) represent a distinct subclass of specialized metabolites predominantly found in the plant kingdom, particularly within the Guttiferae (Clusiaceae) family. These compounds exhibit remarkable structural diversity and a wide range of biological activities. *Seco*- and *nor*-PPAPs, two unique variants of PPAPs with diverse skeletal structures, have been extensively investigated. As of June 2023, 200 compounds have been isolated from four genera, with *Hypericum* being the primary source. Notably, 115 of these compounds were identified in the past four years, indicating a significant increase in research activity. *Seco*- and *nor*-PPAPs can be categorized into six main subgroups based on the original PPAP scaffolds. Biological studies have revealed their potential in various therapeutic applications, including anti-cancer, anti-inflammatory, hepatoprotective, anti-Alzheimer's disease (anti-AD), multidrug resistance (MDR) reversal, anti-depressant, neuroprotective, and immunosuppressive effects. This review provides a comprehensive overview of the occurrence, structures, and bioactivities of natural *seco*- and *nor*-PPAPs, offering valuable insights for the further development of PPAPs.

1. Introduction

Polycyclic polyprenylated acylphloroglucinols (PPAPs), characteristic secondary metabolites of plants, are primarily derived from the genera *Hypericum* and *Garcinia*. These compounds consist of highly oxygenated acylphloroglucinol-derived cores substituted with multiple isoprene units [1-3]. Over 1000 naturally occurring PPAPs have been reported and can be structurally categorized into three subgroups based on their chemical skeleton characteristics, which are directly related to their biogenesis: (i) bicyclic polyprenylated acylphloroglucinols (BPAPs), (ii) caged PPAPs with adamantane and homoadamantane cores, and (iii) other PPAPs, including spirocyclic PPAPs with an octahydrospiro[cyclohexan-1,5′-indene]-2,4,6-trione core and complex PPAPs derived from intramolecular [4 + 2] cycloaddition between the acylphloroglucinol core and side chains (Fig. 1) [1-4]. The diverse structures and intriguing biological activities of these compounds have garnered significant interest from pharmacologists and synthetic chemists [1, 5-15]. Hyperforin, first isolated from *H. perforatum*, exhibits profound biological applications, notably its anti-depressant activity, which is responsible for the use of *H. perforatum* in treating depression [16-22].

Seco- and *nor*-PPAPs, distinct categories of PPAPs, exhibit unique oxygen or carbon ring structures, which serve as crucial sources of diverse molecular frameworks. These PPAPs demonstrate significant structural variations derived from conventional PPAPs through varying degrees of cleavage or degradation of acylphloroglucinol cores or side chains, followed by rearrangement (Fig. 1). Such structural diversity underpins their wide range of biological activities, including anti-cancer, anti-inflammatory, hepatoprotective, anti-Alzheimer's disease (anti-AD), multidrug resistance (MDR) reversal, anti-depressant, neuroprotective, and immunosuppressive properties [23-26]. As of June 2023, approximately 200 naturally occurring *seco*- and *nor*-PPAPs with multiple skeletal structures have been documented in the literature.

While several general reviews have explored PPAPs with respect to their structural characteristics, bioactivities, and biosynthetic and synthetic methods, these works have predominantly focused on representative PPAPs, with limited attention given to the unique *seco*- and *nor*-PPAP subclasses [1, 3, 5, 6, 27, 28]. In response to this gap, the present review aims to systematically profile the recent advances in the distribution, structural diversity, biological activities, and biosynthetic pathways of naturally occurring *seco*- and *nor*-PPAPs, emphasizing novel skeletons reported between January 1988 and June 2023. For clarity and concise-

* Corresponding author.
E-mail addresses: 10280921@qq.com (Y. Tang); qichangxing@hust.edu.cn (C. Qi); zhangyh@mails.tjmu.edu.cn (Y. Zhang)

https://doi.org/10.1016/S1875-5364(25)60911-3

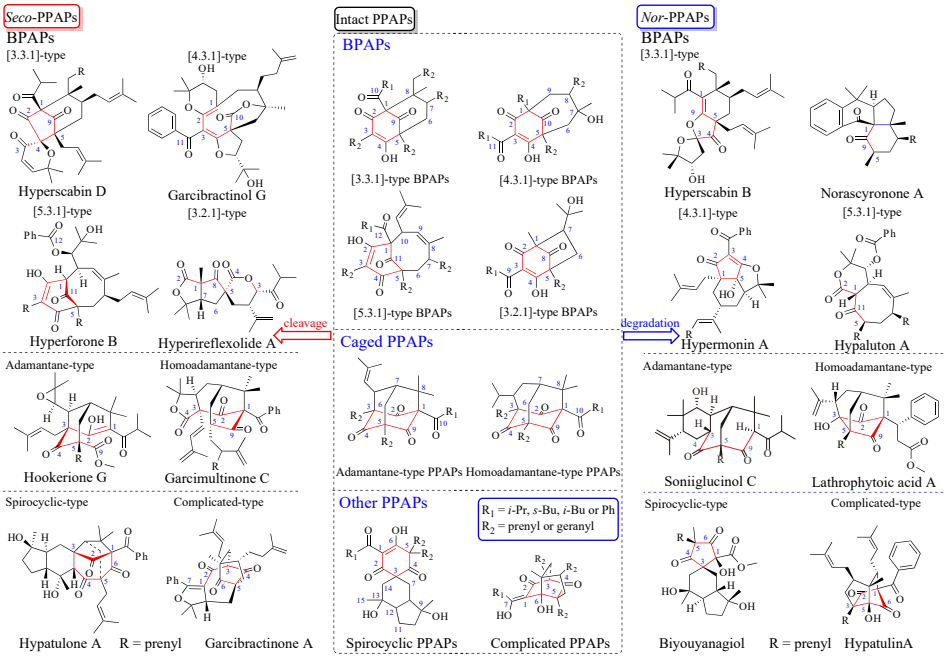

Fig. 1 Classification of PPAPs.

ness, only selected representative structures are highlighted within the main text, while detailed information on all identified structures, their sources, and associated bioactivities is provided in the Supplementary information. This review is intended to serve as a comprehensive reference and to facilitate further research and development efforts focused on these structurally and biologically intriguing PPAP subclasses.

2. Occurrence, classifications, and structures

As of June 2023, a total of 88 *seco*-PPAPs and 112 *nor*-PPAPs, exhibiting diverse skeletal frameworks, have been isolated from 30 plant species belonging to four genera (*Garcinia*, *Hypericum*, *Calophyllum*, and *Kielmeyera*) and two plant families (Clusiaceae and Calophyllaceae) as of June 2023. The majority of these compounds were isolated from the family Clusiaceae, with the exception of lathrophytoic acid A (**182**), which was obtained from the family Calophyllaceae [29]. The genus *Hypericum* was the predominant source, accounting for approximately 90% of the compounds. The aerial parts of plants serve as rich sources of these PPAPs. Notably, 115 of these compounds were discovered within the past four years, reflecting the rapid advancement of phytochemical research. The distribution of these compounds across different plant genera and parts, along with their reported years, is illustrated in Fig. 2 and detailed in Tables S1–S7.

Seco- and *nor*-PPAPs are biosynthetically derived from normal PPAPs (Fig. 1). Their extensive structural variations stem from varying degrees of cleavage or degradation, rearrangements, and cyclization, which have significantly contributed to a diverse and complex array of novel skeletons. These compounds can be categorized into six groups based on the skeletons of normal PPAPs (Fig. 1): *seco*- and *nor*-BPAPs, *seco*- and *nor*-caged PPAPs with adamantane and homoadamantane cores, and *seco*- and *nor*-other (spirocyclic and complicated types) PPAPs. *Seco*- and *nor*-BPAPs and *seco*-spirocyclic PPAPs represent the most common structural types, comprising 24%, 45%, and 14% of the total, respectively (Fig. 3).

Moreover, the proposed biosynthetic pathways suggest that the highly oxygenated acylphloroglucinol-derived cores of typical PPAPs are susceptible to oxidative cleavage or degradation. Additionally, isoprenyl or geranyl side chains may undergo intramolecular cyclization, forming new oxygen or carbon rings. In BPAPs, for instance, bonds such as C-1/C-2, C-1/C-9, C-1/C-10, C-1/C-12, C-2/C-3, C-3/C-4, C-3/C-10, C-4/C-5, or C-5/C-8 in acylphloroglucinols are prone to cleavage and cyclization with side chains, resulting in diverse structures. These can be categorized based on the location of ring splitting and carbon loss, such as 1,2-*seco*, 1,9-*seco*, and 2,3-*seco*-BPAPs. Typically, the C-1/C-2 and C-1/C-9 bonds of the acylphloroglucinol core are common cleavage sites. Further degradation, rearrangement, and cyclization can lead to other novel skeletons, including 2-*nor*, 2,3-*nor*, 2,3,4-*nor*, or 9-*nor* PPAPs. Considering the varying degrees and locations of cleavage, as well as ring formation, it is anticipated that more novel *seco*- and *nor*-PPAPs will be discovered in the future. The hypothetical biogenetic pathways of representative *seco*- and *nor*-PPAPs are summarized (Fig. 4).

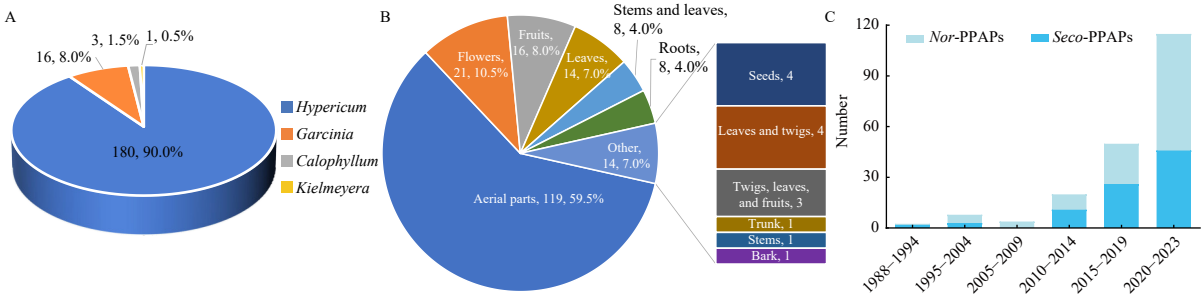

Fig. 2 Distributions of *seco*- and *nor*-PPAPs (A) in genera (B) and plant parts. (C) Number of *seco*- and *nor*-PPAPs reported in the literature up to June 2023.

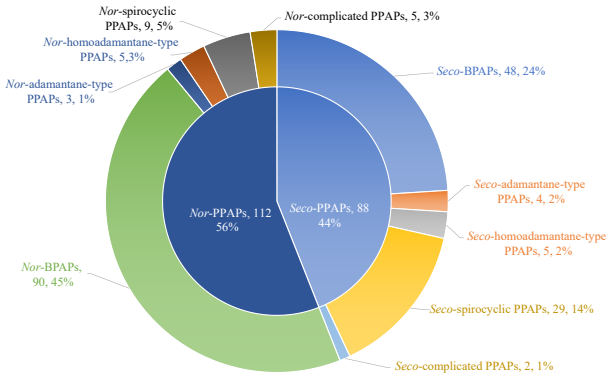

Fig. 3 The proportion of natural *seco*- and *nor*-PPAPs discovered from January 1988 to June 2023.

2.1. Seco-PPAPs

Hyperireflexolides A (**41**) and B (**42**) were initially isolated in 1993, marking the first discovery of *seco*-PPAPs [30]. Subsequently, 88 *seco*-PPAPs have been reported, categorized into three types based on representative PPAP skeletons: *seco*-BPAPs (**1**–**48**, Table S1), *seco*-caged PPAPs with adamantane and homoadamantane core (**49**–**57**, Table S2), and *seco*-other PPAPs (**58**–**88**, Table S3), with *seco*-BPAPs being the most common structures. *Seco*-other PPAPs can be further subdivided into two groups: *seco*-spirocyclic PPAPs (**58**–**86**) and *seco*-complicated PPAPs (**87** and **88**).

2.2. Seco-BPAPs

This class encompasses forty-eight *seco*-BPAPs, categorized into distinct types: *seco*-[3.3.1]-type BPAPs (**1**–**40**), *seco*-[3.2.1]-type BPAPs (**41**–**43**), *seco*-[4.3.1]-type BPAPs (**44** and **45**), and *seco*-[5.3.1]-type BPAPs (**46**–**48**). The majority of these compounds are hypothesized to originate from BPAPs containing a bicyclo[3.3.1]nonane-2,4,9-trione core. Their diverse structures (**1**–**40**) are likely formed through the cleavage of specific bonds (C-1/C-2, C-1/C-9, C-2/C-3, C-3/C-4, or C-3/C-10) and subsequent rearrangement (Fig. 4) [1].

Garcinielliptone G (**1**) and hyperscabin D (**2**), 2,3-*seco*-BPAPs featuring a distinctive bicyclo[3.2.1] octane skeleton, are hypothesized to originate from the cleavage of the C-2/C-3 bond in the acylphloroglucinol core of BPAPs containing a bicyclo[3.3.1]nonane-2,4,9-trione core [31, 32]. Furthermore, hypsampsone A (**3**) was characterized *via* oxidative cleavages of the C-2/C-3 and C-3/C-4 bonds of BPAPs, followed by a rearrangement that led to the formation of a spirocyclic system with a distinctive 5/6/5/5 tetracyclic skeleton (Fig. 5) [33].

Fifteen 1,9-*seco*-BPAPs (**4**–**18**) featuring a distinctive eight-membered carbon ring connected to a five-membered lactone ring were isolated from the *Hypericum* family. These compounds likely originated through the cleavage of the C-1/C-9 bond at the acylphloroglucinol core of BPAPs. A comprehensive chemical investigation of *H. henryi* yielded hyphenrones A–D (**4**, **5**, **16**, and **18**), H (**6**), and I (**17**) [34, 35]. **16**–**18** exhibit unique 5/8/5 or 6/6/5/8/5 ring systems formed through an additional intramolecular cyclization of side chains (Fig. 6) [34, 35]. The structure of perforatumone was ultimately revised to **4** through biomimetic transformation [35, 36]. Additionally, the structure of attenuatumione B (**11**), initially isolated from *H. attenuatum*, was corrected to 1,9-*seco*-BPAP by nuclear magnetic resonance (NMR) spectroscopic analysis, revealing the same skeleton as **4** and **5** [37, 38]. Five novel 1,9-*seco*-BPAPs (**19**–**23**) likely derived from multiple cleavages and rearrangement of BPAPs. Hyperfol A (**19**) is hypothesized to form *via* the oxidative cleavage of C-1/C-9 and C-2/C-3 bonds, subsequently rearranging to form the fused 5/5/9/5 tetracyclic skeleton, as determined by NMR, electronic circular dichroism (ECD) analyses, and computer-assisted structure elucidation software (Fig. 6) [39]. Structurally, ascyronones A (**20**) and B (**21**), and hyperforcinols E (**22**) and K (**23**) share an unusual seven-membered carbon core fused to a *γ*-lactone ring, likely formed by 1,9-*seco*-BPAPs through further cleavage of the C-2/C-3 bond (Fig. 6) [40, 41]. Furthermore, biomimetic transformation elucidated the structure of **20**. The absolute structure of **23** was revised by comparing its ECD data with that of **22** [41, 42].

Eight 1,2-*seco*-BPAPs (**24**–**36**) with seven distinct skeletons were isolated from [3.3.1]-type BPAPs through C-1/C-2 bond cleavage and rearrangement (Fig. 4). Among these, hyperhexan-

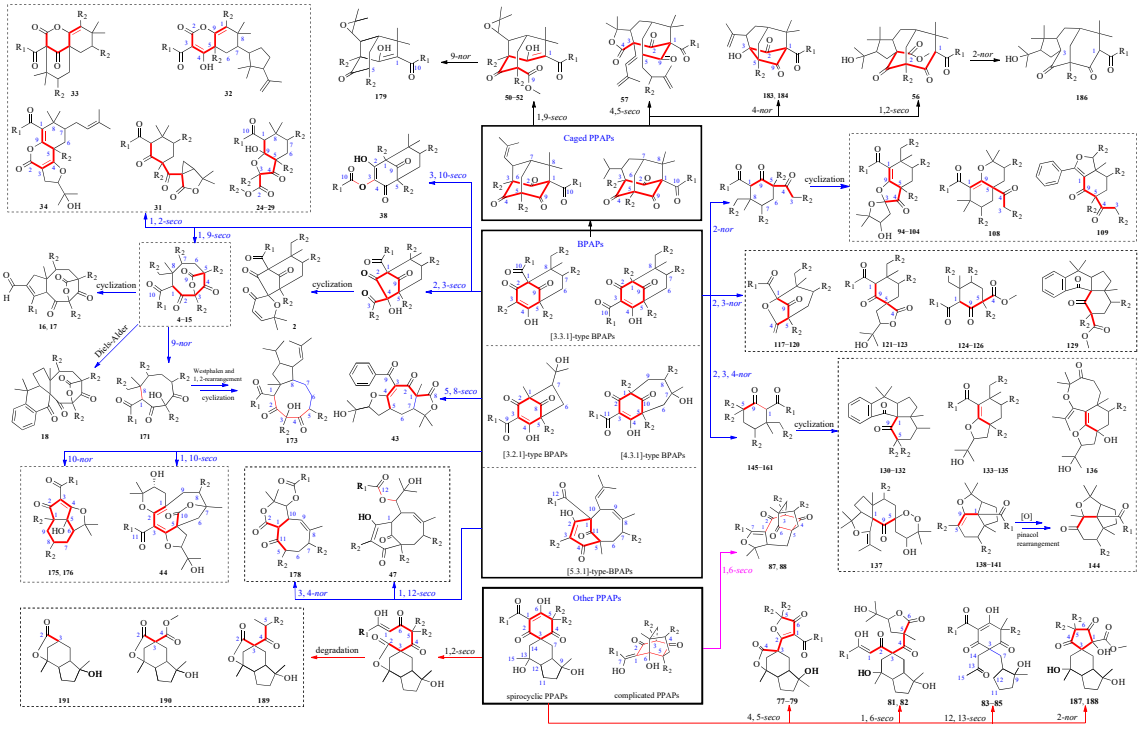

Fig. 4 Hypothetical biogenetic pathways of representative *seco*- and *nor*-PPAPs.

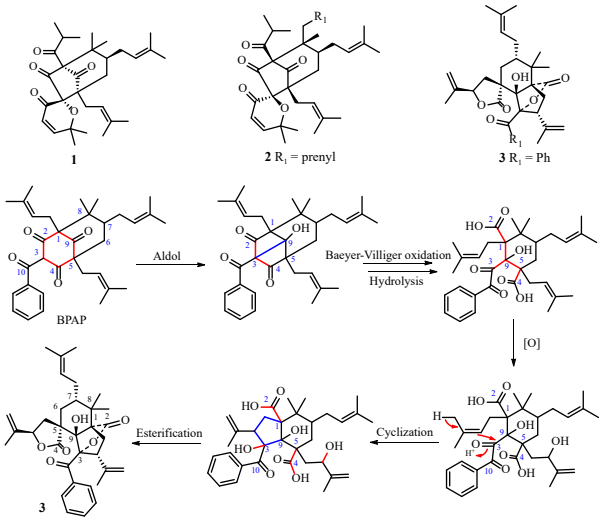

Fig. 5 Structures of **1**–**3** and possible biosynthetic pathway of **3**.

ones A (**24**) and F (**25**) [33, 43], hyperacmosin M (**26**) [44], hyperforcinol D (**27**) [41], and hyperacmosins C (**28**) and D (**29**) share an octahydrobenzofuran system skeleton [45], extracted from *H. sampsonii*, *H. acmosepalum*, or *H. forrestii*. Hyperbenzones A (**30**) and B (**31**), isolated from *H. beanii* roots, exhibit a 6/5/5 spirocyclic system and an unusual 3-oxabicyclo[3.1.0]hexan-2-one moiety, respectively. These structures are hypothesized to form *via* retro-Claisen reaction and cyclization (Fig. 7). The structure of **30** was conclusively determined through DP4+ calculation, crystallographic analysis, and ECD studies [46].

Thoreliolides A (**32**) and B (**33**) were isolated from the fruits of *Calophyllum thorelii*, exhibiting a distinctive hexacyclic-fused six-membered lactone ring system [47]. Hypsampsonione A (**34**), characterized by an octahydro-2*H*-chromen-2-one framework, was elucidated *via* comprehensive spectroscopic analyses and quantum chemistry calculations [48].

The 3,10-*seco*-BPAPs are proposed to arise from BPAPs *via* the Baeyer–Villiger reaction at the C-3 side chain, leading to structural cleavage. To date, four novel 3,10-*seco*-BPAPs (**37**–**40**) have been identified. Paucinone C (**37**), the first member of this subclass, possesses a cyclohexane-spiro-tetrahydrofuran moiety and was isolated from the leaves of *G. paucinervis* in 2010 [49]. Oblongifolin M (**38**) [50], hyperascyrin N (**39**) [51], and compound **40**, all exhibiting a tricyclo-[4.3.1.1^{1,4}]-undecane skeleton [52], were obtained from *G. oblongifolia*, *H. ascyron*, and *H. scabrum*, respectively.

Three novel compounds (**41**–**43**) derived from [3.2.1]-type BPAPs have been identified. Hyperireflexolides A (**41**) and B (**42**), a pair of epimers characterized by a 5/5/6 system with dilactone rings, were initially isolated from *H. reflexum*. The structure of **41** was confirmed through X-ray analysis, while **42** was subsequently revised and defined *via* a bioinspired total synthesis [30, 53]. Furthermore, George's group reported that **41** and **42** were derived from the significant precursor enaimeone A [54], a bicyclo[3.2.1]octane PPAP natural product, through the cleavages of C-2/C-3 and C-3/C-4 bonds, and rearrangement based on their biosynthetic pathway (Fig. 8) [7]. This work represents the first discovery of *seco*-[3.2.1]-type BPAPs. Compound **43**, isolated from *H. scabrum* [52], possesses a cycloheptane ring fused to furan and γ-lactone rings and was generated from BPAP through the cleavage of the C-5/C-8 bond (Fig. 8). The structure of **43** was successfully elucidated by X-ray analysis [30].

Garcibractinols G (**44**) and H (**45**), two uncommon *seco*-

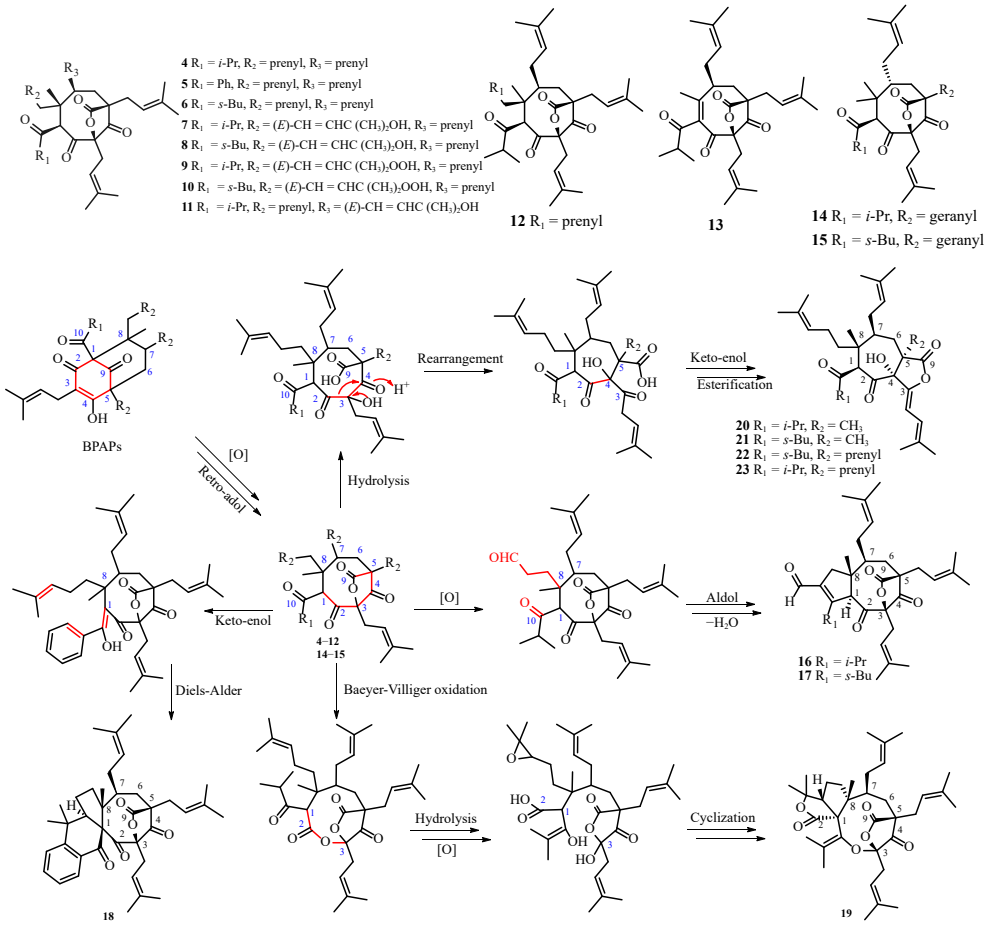

Fig. 6 Structures of **4**–**15** and possible biosynthetic pathway of **4**–**12**, **14**–**23**.

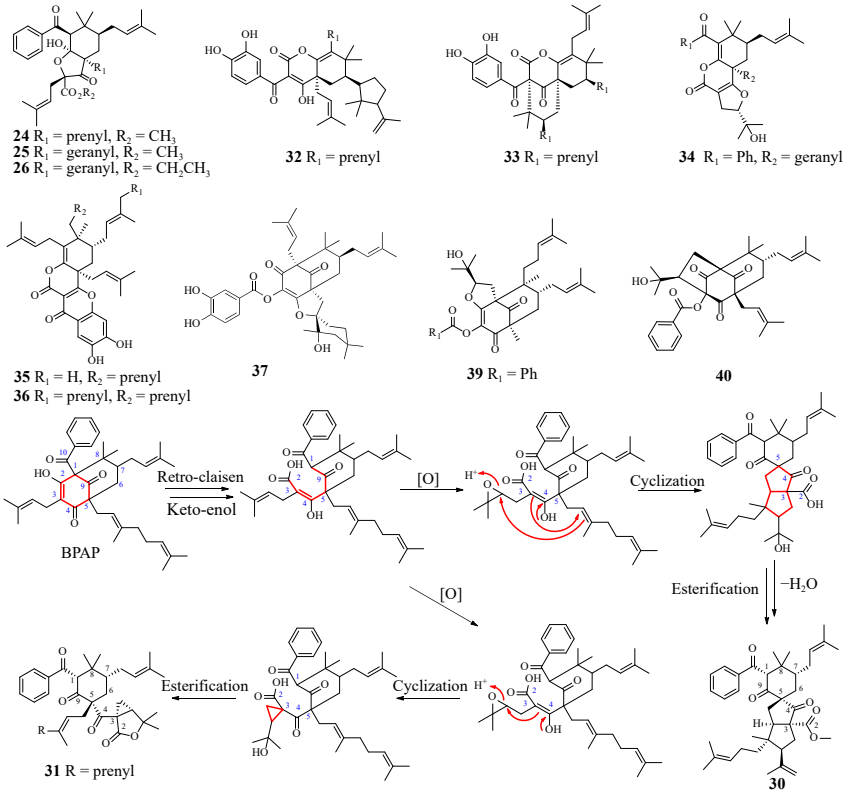

Fig. 7 Structures of **24–26**, **32–37**, **39–40** and possible biosynthetic pathways of **30–31**.

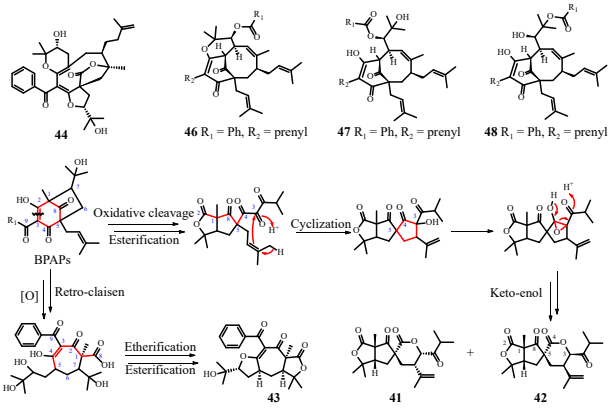

Fig. 8 Structures of **44**, **46–48** and possible biosynthetic pathways of **41–43**.

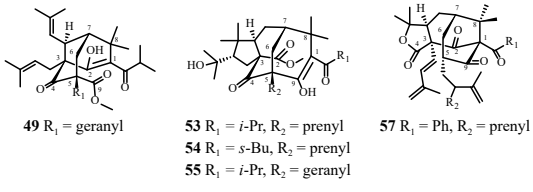

Fig. 9 Structures of **49**, **53–55**, and **57**.

[4.3.1]-type BPAPs, were isolated from the fruits of *G. bracteate*. These compounds result from the cleavage of the C-1/C-10 bond, which opens the acylphloroglucinol ring through a retro-Claisen reaction (Fig. 4) [55].

Hyperforones A–C (**46–48**), three novel compounds obtained from *H. forrestii*, represent the first examples of benzoyl-migrated [5.3.1]-type BPAPs, classified as 1,12-*seco*-[5.3.1]-type BPAPs (Fig. 4) [56]. From a biosynthetic perspective, **47** is hypothesized to be the precursor of **46** and **48** [56].

2.3. Seco-caged PPAPs with adamantane and homoadamantane cores

Seco-caged PPAPs were hypothesized to originate from PPAPs with adamantane (tricyclo[3.3.1.1]decane) and homoadamantane (tricyclo[4.3.1.1]undecane) cores (Fig. 4). Four novel 1,9-*seco*-adamantane-type PPAPs, namely hypersubone A (**49**) (Fig. 9)[57], and hookeriones E–G (**50–52**), were isolated from *H. subsessile* or *H. hookerianum* [58]. **49** represents the first identified member of 1,9-*seco*-adamantane-type PPAPs, featuring a tetracyclo-[6.3.1.$1^{3,10}$.$0^{4,8}$]-tridecane core. Additionally, biomimetic synthesis was employed to determine the absolute configurations of **50–52** [58].

Four 1,2-*seco*-homoadamantane-type PPAPs, hypersonins A–D (**53–56**) (Fig. 9), were isolated from *H. wilsonii*. These compounds feature a novel bicyclo[4.3.1]decane-3-methoxycarbonyl structure [59]. The absolute configuration of **53** was elucidated through X-ray crystallography [59]. Additionally, garcimultinone C (**57**) (Fig. 9), the first reported 4,5-*seco*-homoadamantane-type PPAPs, exhibiting a 5-oxatricyclo[7.3.1.$0^{3,7}$]tridecane skeleton, was extracted from *G. multiflora* [60].

2.4. Seco-other PPAPs

Twenty-nine *seco*-spirocyclic PPAPs (**58–86**) and two *seco*-complicated PPAPs (**87** and **88**) are described. From a biogenetic perspective, *seco*-spirocyclic PPAPs likely originate from spirocyclic PPAPs with an octahydrospiro[cyclohexan-1,5′-indene]-2,4,6-trione core through the cleavage of C-1/C-2, C-1/C-6, C-3/C-4, C-4/C-5, C-12/C-13, or C-13/C-14 bonds, followed by cyclization and rearrangement to form new skeletons (Fig. 4). Complicated PPAPs, resulting from intramolecular [4 + 2] cycloaddition between the acylphloroglucinol core and side chains, potentially undergo oxidative cleavage and reconstruction to form new oxygen or carbon rings (Fig. 4).

Six 3,4-*seco*-spirocyclic PPAPs have been identified. Hypatulone A (**58**), featuring a novel skeleton, was isolated from *H. patu-*

lum [61]. Its structure was subsequently revised and confirmed through NMR analysis, biogenetic pathway examination, and quantum chemical calculations by Grossman's research team [62]. **58** represents the first 3,4-*seco*-spirocyclic PPAP, characterized by a unique 5/6/6/6/5 ring system [62]. The proposed biosynthetic pathway suggests that Paternò-Büchi reaction, nucleophilic attack, and aldol reactions could be key steps, as illustrated in Fig. 10. Hymoins C (**59**) and D (**60**), sharing the same skeletal structure, were isolated from *H. monogynum* [63]. Hyperberlone A (**61**), isolated from *H. beanii*, features a rare tricyclo[4.3.1.0^{3,8}]decane core. It possessed an interesting caged tricyclic 6/6/5 ring system similar to **58**–**60** (Fig. 10) [64]. Spihyperglucinols C (**62**) and D (**63**) contain an unexpected bicyclo[3.2.2]nonane core, with a proposed biosynthetic pathway depicted in Fig. 10 [65].

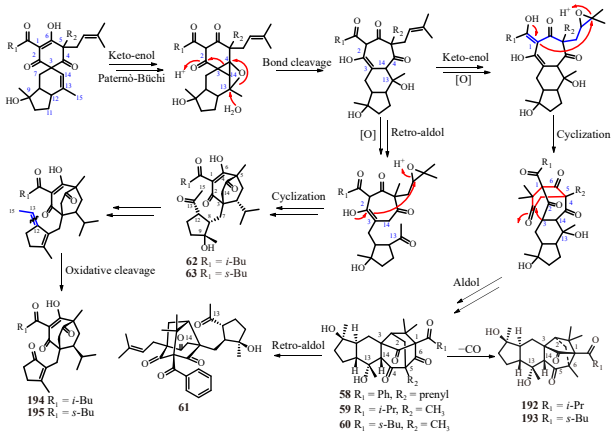

Fig. 10 Possible biosynthetic pathways of **58**–**63** and **192**–**195**.

To date, eleven novel 1,2-*seco*-spirocyclic PPAPs (**64**–**76**) with four distinct skeletons have been reported, and their proposed biosynthetic pathways are illustrated in Fig. 11. Compounds **64**–**68** exhibit a characteristic five-membered dilactone motif, originating from the cleavage of the C-1/C-2 bond of typical spirocyclic PPAPs *via* retro-Claisen reaction, followed by cyclization, keto-enol tautomerization, esterification, and stereospecific photoisomerization reactions. Biyoulactones A–C (**64**–**66**), isolated from *H. chinense*, represent the first discovered 1,2-*seco*-spirocyclic PPAPs [66], while hypemoins A (**67**) and B (**68**) were isolated from *H. monogynum* [67]. Hypermononones A–D (**69**–**72**), four new 1,2-*seco*-spirocyclic PPAPs featuring single *δ*-lactone and tricyclic *γ*-lactone moieties [68], and hybeanones A (**73**) and B (**74**), containing a cyclopentanone unit fused to a tricyclic *γ*-lactone unit *via* a ketone carbonyl, were isolated from *H. beanii*. Their proposed biosynthetic pathway involves key photoisomerization or Baeyer-Villiger oxidation steps (Fig. 11) [69]. The structures of **64**, **67**, **69**, and **73** were confirmed through X-ray diffraction analysis. Furthermore, hunascynols A (**75**) and B (**76**) represent the first instances of direct acylphloroglucinol core-opening spirocyclic PPAPs without subsequent cyclization (Fig. 11) [70].

Five 4,5-*seco*-spirocyclic PPAPs (**77**–**80**) are examined (Fig. 4). Furanmonogones A (**77**) and B (**78**), featuring a 4,5-*seco*-3(2*H*)-furanone motif, were isolated from *H. monogynum* [71]. Subsequently, Yang's group reported the first total synthesis of their deacylation products, further validating their skeletal structure [72]. Hyperhenone M (**79**), obtained from *H. henryi*, exhibited the same skeletal structure as **77** and **78** [73]. Hyperbeanone A (**80**), characterized by a benz[*f*]indene-1,9(4*H*)-dione ring system, was isolated from *H. beanii* [74]. Its carbon skeleton is hypothesized to form through the cleavage of the C-4/C-5 bond and a Diels-Alder reaction based on the intact spirocyclic PPAP (Fig. 11).

Biyoulactones D (**81**) and E (**82**), two novel 1,6-*seco*-spirocyclic PPAPs, featuring a unique *γ*-lactone ring, were initially isolated from *H. chinense* in 2012 [75]. Hyperilongenols A–C (**83**–**85**),

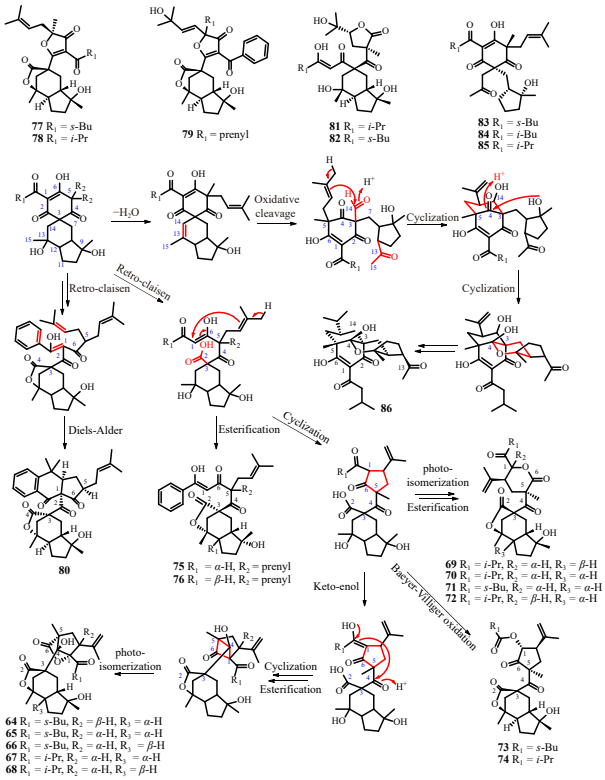

Fig. 11 Structures of **77**–**79**, **81**–**85** and possible biosynthetic pathways of **64**–**76**, **80**, **86**.

the first naturally occurring 12,13-*seco*-spirocyclic PPAPs with an enolizable *β*,*β*′-tricarbonyl system, were extracted from *H. longistylum*. **83** existed as a mixture of inseparable configurational isomers of *iso*-butyryl in solid crystals, while a suitable crystal of **83** confirmed its structure [76]. Further analysis of *H. longistylum* yielded three unusual 13,14-*seco*-spirocyclic PPAPs, including longisglucinol A (**86**) [77]. The structure of **86**, possessing an unprecedented 6/6/6/5 core as the first representative of this subgroup, was verified by X-ray analysis. Its potential biosynthetic pathway, involving oxidative cleavage and a series of cyclization reactions, is illustrated in Fig. 11.

Garcibractinones A (**87**) and B (**88**), two rare *seco*-complicated PPAPs, were isolated from *G. bracteate*, exhibiting a caged tricyclo-[4.4.1.1^{1,4}]dodecane skeleton. These compounds likely originate from nemorosonol or doitunggarcinone B *via* C-1/C-6 bond cleavage, followed by intramolecular cyclization of the side chains at C-1 and C-5 (Fig. 12) [14, 78-81]. The structure of **87** was determined through comprehensive spectroscopic analysis and single-crystal X-ray diffraction [78].

2.5. *Nor*-PPAPs

Nor-PPAPs are derived through various degrees of carbon loss occurring in the side chain or *seco*-rings [1, 23, 25]. Since the ini-

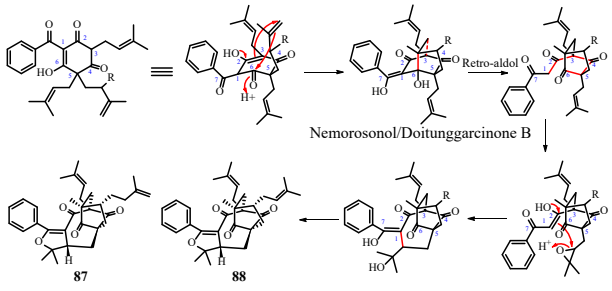

Fig. 12 Possible biosynthetic pathways of **87** and **88**.

tial discovery of soulattrone A (**117**) from the bark of *C. soulattri* in 1988 [82], 112 *nor*-PPAPs (**89–200**) have been identified. These compounds can be categorized into three groups: *nor*-BPAPs (**89–178**), *nor*-caged PPAPs with adamantane and homoadamantane cores (**179–186**), and *nor*-other PPAPs (**187–200**). *Nor*-BPAPs constitute the primary category of these compounds, exhibiting diverse structures and representing 45% of the summarized review (Fig. 3). Consequently, their proposed biosynthetic pathways have been the most extensively described in the literature.

2.6. Nor-BPAPs

Ninety *nor*-BPAPs, primarily derived from [3.3.1]-type BPAPs through degradation of C-2, C-2/C-3, C-2/C-3/C-4, or C-9 (including the side chain at C-3) (**89–174**), are described (Fig. 4). Compounds **175–177** originate from [4.3.1]-type BPAPs, while hypaluton A (**178**) stems from [5.3.1]-type BPAP.

Twenty-eight new 2-*nor*-BPAPs (**89–116**) exhibiting eleven distinct skeletal structures were identified through the absence of the C-2 carbonyl group in the acylphloroglucinol ring of conventional BPAPs (Fig. 4).

Norsampsones A–D (**89–92**) were the first identified 2-*nor*-BPAPs [26]. Xu's group initially reported the total synthesis pathways of **89** and **90** to further confirm their structures [83]. **94–104** share an identical skeleton with a unique hexacyclic-fused 1,6-dioxaspiro[4.4]nonane core and were isolated from *H. scabrum*, *H.patulum*, or *H. acmosepalum* in recent years. X-ray crystallographic data identified norhyperpalums B (**99**) and A (**104**) [24]. Hypericumoxide N (**105**) [84], hyperpatone A (**106**) [85], and hyperacmosin R (**107**) exhibit a similar 6/5 skeleton, formed through key Baeyer-Villiger oxidative, decarbonylation, and intramolecular cyclization of the side chains at C-1 and C-8. Their oxygen ring systems were generated *via* a series of oxidation and intramolecular cyclization reactions (Fig. 13). Notably, **106** contains an intramolecular peroxy bridge with a rare 8/6/5/6/5 system, while **107** includes a 5,8-spiroketal subunit [86]. Norgarmultinone B (**108**) and norwilsonnol B (**109**) feature a cyclohexane ring fused to a pyran or furan ring [87,88]. Extensive phytochemical study of *H. perforatum* revealed three novel hyperforones F–H (**110–112**), possessing a rare macrocyclic lactone ring, presumed to form *via* the key oxidative cleavage of the C-3/C-4 bond to open the ring (Fig. 14). X-ray diffraction analysis confirmed the absolute configuration of **110** [89]. Investigation of *H. przewalskii* led to the isolation and characterization of norprzewalsone A (**113**), featuring a new 5/6/5/6/6 pentacyclic ring system [90], potentially originating from typical BPAP through C-2 degradation and secondary cyclization, including a Diels-Alder reaction between the side chains at C-1 and C-8 (Fig. 14).

Hypersampones A–C (**114–116**) represent the first *nor*-PPAPs exhibiting a tetracyclic 6/5/5/6 ring system. This unique skeletal structure is hypothesized to result from isopentenyl cyclase catalysis of intact BPAPs, followed by retro-Dieckmann reaction and decarboxylation (Fig. 14). Compounds **114** and **115** were presumably formed through C-1/C-10 bond cleavage and rearrangement from **116**. The structural elucidation of **114** was confirmed *via* X-ray crystallography [91].

2,3-*Nor*-BPAPs may undergo loss of C-2, C-3, and the side chain at C-3, followed by cyclization and rearrangement to form diverse skeletons (Figs. 4 and 15). Thirteen novel 2,3-*nor*-BPAPs (**117–129**) have been reported. Soulattrone A (**117**), the first member of this subgroup isolated from *C. soulattri*, features a cyclohexane fused to *γ*-lactone, as determined *via* NMR data and X-ray crystallographic evidence [82]. Garcinielliptone J (**118**) [31], and norhyperpalums F (**119**) and G (**120**) share the same skeleton as **117** [24]. Norhyperpalum H (**121**) [24], and spirohypolactones A

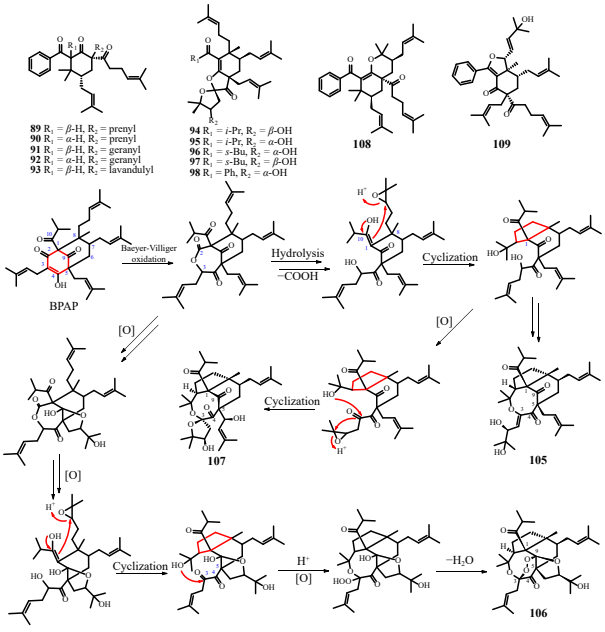

Fig. 13 Structures of **89–98**, **108**, **109** and possible biosynthetic pathways of **105–107**.

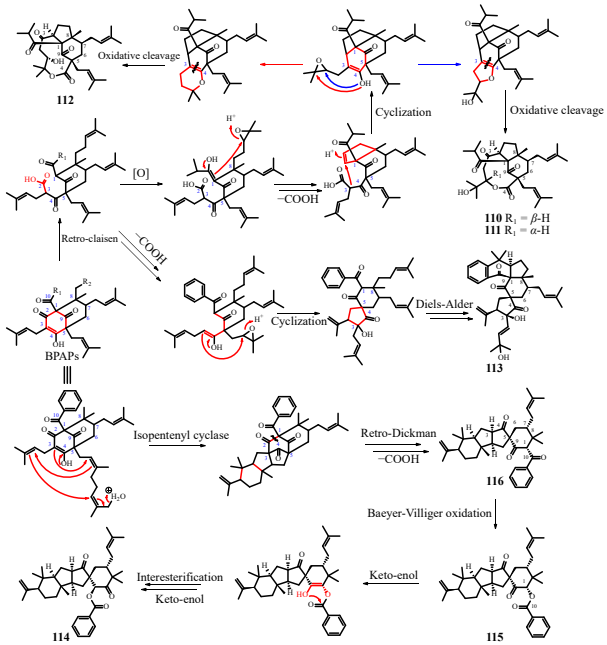

Fig. 14 Possible biosynthetic pathways of **110–116**.

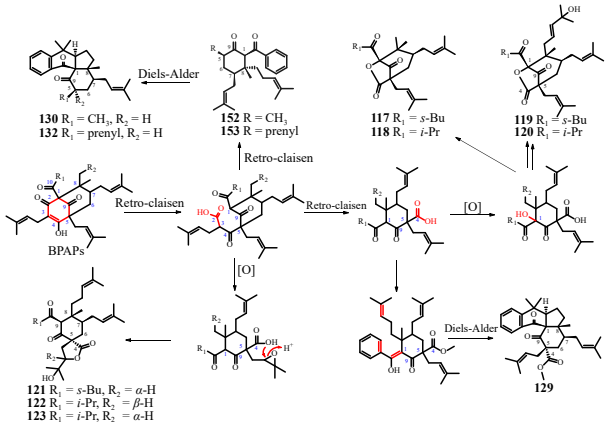

Fig. 15 Possible biosynthetic pathways of **117–123**, **129**, **130**, **132**, **152**, and **153**.

(**122**) and B (**123**) [92], isolated from *H. patulum* or *H. perforatum*, possess the 2-oxaspiro[4.5]decane spirocyclic skeleton. Compounds **124**–**128** exhibit the same cyclohexane monocyclic system, and the absolute structure of garcinielliptone O (**127**) was established through total synthesis [83]. A chemical investigation of *H. pseudohenryi* identified hypseudohenrin A (**129**) with a unique 6/5/6/6 ring system [93], which likely formed biogenetically *via* key retro-Claisen and Diels-Alder reactions (Fig. 15).

Forty-one 2,3,4-*nor*-BPAPs (**130**–**170**) exhibiting diverse skeletal structures have been identified. In comparison to 2,3-*nor*-BPAPs, the defining structural characteristic of this subgroup is the degradation at the C-4 position (Fig. 4).

Norascyronones A (**130**) and B (**131**) represent the first instances of 2,3,4-*nor*-BPAPs exhibiting the same carbon skeleton as **129**. Their structures were confirmed through X-ray diffraction data and total or biomimetic synthesis [23, 94-96]. Hypseudohenrin B (**132**) shares a similar skeleton to **130** [93]. Seven novel compounds (**138**–**144**) were isolated from *H. yezoense* or *H. monogynum*, comprising 6/5 carbon rings fused to a furan ring [97, 98]. These compounds were formed through the degradation of C-2/C-3/C-4 and intramolecular cyclization (Fig. 16). The structures of yezo'otogirin A (**138**) and C (**140**), and hypermogin D (**144**) were elucidated *via* biomimetic synthesis [95, 99-101].

Since **151** was obtained from *H. perforatum* in 2001 as the first 2,3,4-*nor*-BPAP with a cyclohexane monocyclic ring [102, 103], eighteen analogous compounds (**145**–**162**) have been reported. The structures of hyperibrin B (**146**), and hyperscabrones H (**148**) and I (**149**) were revised through biosynthetic methods, NMR analysis, and chemical synthesis [68, 104-106]. X-ray crystallography confirmed the structure of hypermonone H (**147**) [68]. Hyperibrin A (**145**), garcinielliptone N (**150**), and hyperscabrin A (**157**) were successfully synthesized, validating their absolute structures [83, 95, 107]. Phytochemical investigation of *H. perforatum* by Zhang's group yielded a series of 2,3,4-*nor*-BPAPs: hyperhexanones C–E (**134**–**136**) [92], hyperforones A–E (**163**–**167**), I (**168**) and J (**170**) with nine novel skeletons [89]. A plausible biosynthetic pathway for **163**–**170** was proposed, with key steps potentially involving retro-Claisen, intramolecular cyclization, oxidative cleavage, and aldol reactions (Fig. 16). Notably, hyperforones A–C (**163**–**165** and **46**–**48**) were reported with identical names but different structures. Norhyperpalum I (**133**) [24], norwilsonnol A (**137**) [88], and norprzewalsone B (**169**) [90] were obtained from *H. patulum*, *H. wilsonii*, or *H. przewalskii*, respectively, by the same research group. X-ray diffraction analysis confirmed the structures of **137**, **163**, **168**, and **170**.

The distinctive feature of 9-*nor*-BPAP (**171**–**174**) is the absence of C-9 in comparison to [3.3.1]-type BPAPs (Fig. 4). Hyphenrone F (**171**), the inaugural 9-*nor*-BPAP, contains an eight-membered carbon ring, potentially derived from **4** *via* decarbonylation (Fig. 17). Its structure was confirmed through X-ray diffraction analysis [34]. Ascyronone C (**172**), isolated from *H. ascyron*, shares the same skeletal structure as **171** [40]. A bioassay-guided investigation of *H. perforatum* using UPLC-Q-Orbitrap-MS/MS led to the isolation of hyperforen A (**173**), the first PPAP exhibiting a bicyclo[7.3.0]dodecane core and the largest carbon ring [108]. Uralin B (**174**), extracted from *H. uralum*, features a five-membered carbon ring. From a biogenetic perspective, **171**, serving as a precursor, underwent a crucial Westphalen rearrangement for ring expansion, followed by Wagner-Meerwein rearrangement and cyclization between the two prenyl groups to form the 9/5 ring system. Conversely, **174** may have evolved from **171** through the loss of C-2/C-3/C-4 and the side chain at C-3, followed by oxidation and cyclization processes (Fig. 17) [109].

Hypermonins A (**175**) and B (**176**), a pair of isomers at C-5, exhibit a decahydroindeno[1,7-*bc*]furan ring system, derived from the [4.3.1]-type BPAPs through the loss of C-10 and subsequent cyclization (Fig. 18). These compounds represent the first examples of *nor*-[4.3.1]-type BPAPs [110]. Garciyunnanin G (**177**), isolated from *G. yunnanensis*, also belongs to this group [111]. Hypaluton A (**178**), obtained from *H. patulum*, is the first known degradation product of [5.3.1]-type BPAP. Its biosynthesis occurs through the degradation of C-3 and C-4 based on the [5.3.1]-type BPAP structure (Fig. 18) [25].

2.7. Nor-caged PPAPs with adamantane and homoadamantane cores

These classes of *nor*-PPAPs originate from caged PPAPs with adamantane and homoadamantane cores *via* processes of decarbonylation and structural reconstruction (Fig. 4).

The eight reported compounds (**179**–**186**) are categorized into two distinct subgroups (Fig. 19): *nor*-adamantane-type PPAPs (**179**–**181**) and *nor*-homoadamantane-type PPAPs (**182**–**186**).

Hookerione H (**179**), isolated from *H. hookerianum*, represents the first characterized compound in this group exhibiting the adamantane-type PPAP skeleton through the loss of C-9 (Fig. 4) [58]. Soniiglucinols C (**180**) and D (**181**) (Fig. 19), two 2-*nor*-adamantane-type PPAPs, were isolated from *H. wilsonii* [112].

Lathrophytoic acid A (**182**) [29], norsampsone E (**183**) [113], hy-

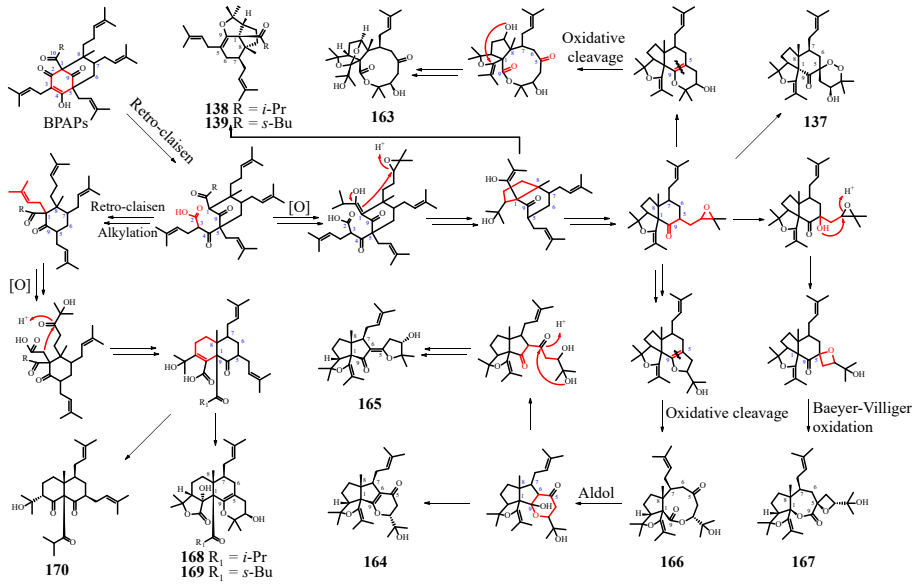

Fig. 16 Possible biosynthetic pathways of **137**–**139** and **163**–**170**.

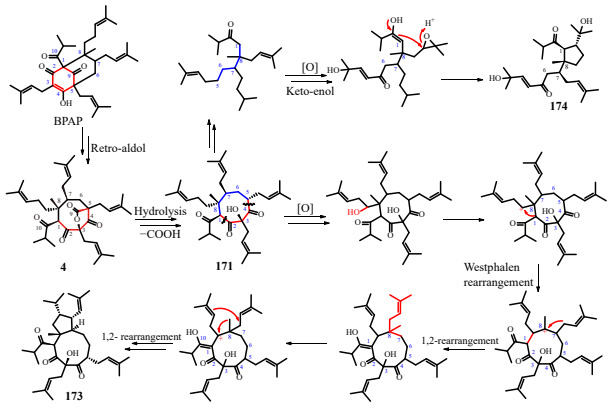

Fig. 17 Possible biosynthetic pathways of **4**, **171**, **173**, and **174**.

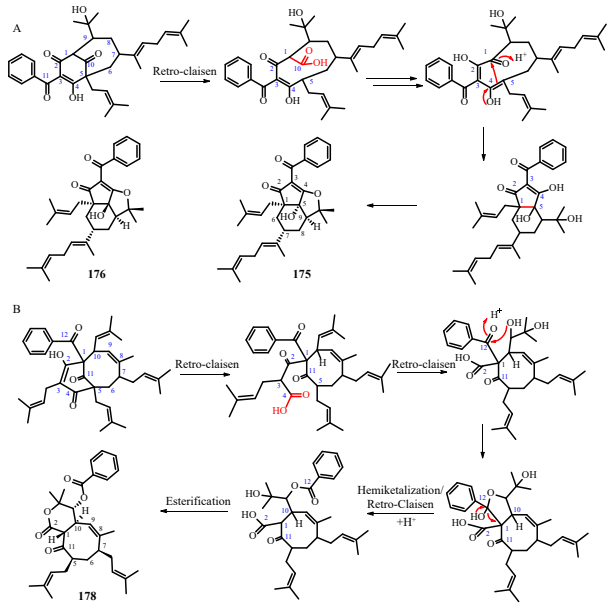

Fig. 18 Possible biosynthetic pathways of **175**, **176**, and **178**.

peracmosin E (**184**) [114], and soniiglucinol A (**185**) [112], were formed *via* the loss of C-4 based on homoadamantane-type PPAPs. **182**–**184** exhibit an unusual caged carbon skeleton featuring a 1,3-dione-4-cyclopentanol moiety, while soniiglucinol A (**185**) presents an atypical 5/7/6 carbon skeleton. Furthermore, soniiglucinol B (**186**) represents the first identified 2-*nor*-homoadamantane-type PPAP [112]. The structures of **180** and **185** were confirmed *via* single-crystal X-ray diffraction analysis.

2.8. Nor-other PPAPs

Nor-spirocyclic PPAPs (**187**–**195**) and *nor*-complicated

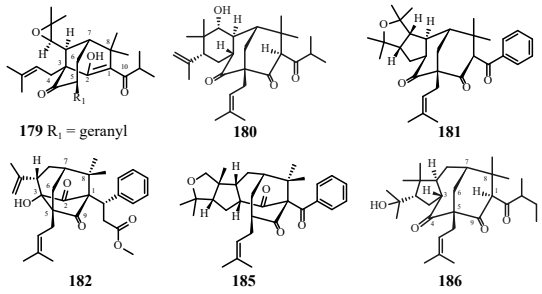

Fig. 19 Structures of **179**–**182**, **185**, and **186**.

PPAPs (**196**–**200**) are categorized according to their structural features and hypothesized biosynthetic routes (Fig. 1).

Biyouyanagiol (**187**), the first example of *nor*-spirocyclic PPAPs, likely originates from typical spirocyclic PPAP through the loss of C-2 *via* Baeyer-Villiger oxidation and decarbonylation, followed by cyclization, forming a unique cyclopenta-1,3-dione moiety (Fig. 20) [115]. Another novel 2-*nor*-spirocyclic PPAPs, uralin D (**188**) [109], was isolated from *H. uralum*.

Investigations into the chemical composition of *H. monogynum* flowers yielded three previously undescribed oxidative degradation spirocyclic PPAPs, hypemoins C–E (**189**–**191**) [67], as well as hymoins A (**192**) and B (**193**), which possess a rare caged pentacyclic 5/6/6/5/5 structure [63]. Compounds **192** and **193** are hypothesized to be C-6 degradation products of **59** and **60**, respectively, potentially resulting from light-induced transformation in the proposed biosynthetic pathway (Fig. 10). The structural configuration of **192** was further confirmed through X-ray crystallography analysis.

Spihyperglucinols A (**194**) and B (**195**), two novel 13,15-*nor*-spirocyclic-type PPAPs isolated from *H. longistylum* [65], are likely derived from the loss of C-13 and C-15 in two 13,14-*seco*-spirocyclic PPAPs, **62** and **63** (Fig. 10). The absolute configuration of **194** was determined through single-crystal X-ray diffraction analysis [65].

Five novel *nor*-complicated PPAPs (**196**–**200**) were isolated from *H. patulum* or *H. forrestii*. Three 4-*nor*-complicated PPAPs, hypatulins A (**196**) and B (**197**) [116], and hyperforcinol C (**198**) [41], were identified. Structurally, **196** and **198**, a pair of isomers, feature a unique tricyclic octahydro-1,5-methanopentalene core. Biogenetically, **196** may be formed through intramolecular cyclization, oxidation, ring cleavage of the C-3/C-4 bond, and cyclization associated with decarboxylation of a plausible biogenetic precursor, a monocyclic polyprenylated acylphloroglucinol (MPAP). Compound **197**, possessing a bicyclo[3.2.1]octane moiety, might be produced by oxidative cleavage of the C-1/C-6 bond based on precursor **196**, followed by methylation (Fig. 21). Additionally, Christmann's group reported a total synthesis of 3-*epi*-hypatulin B, highlighting the use of flow chemistry to enable challenging late-stage transformations in natural product synthesis [117]. An extensive chemical investigation of *H. patulum* yielded

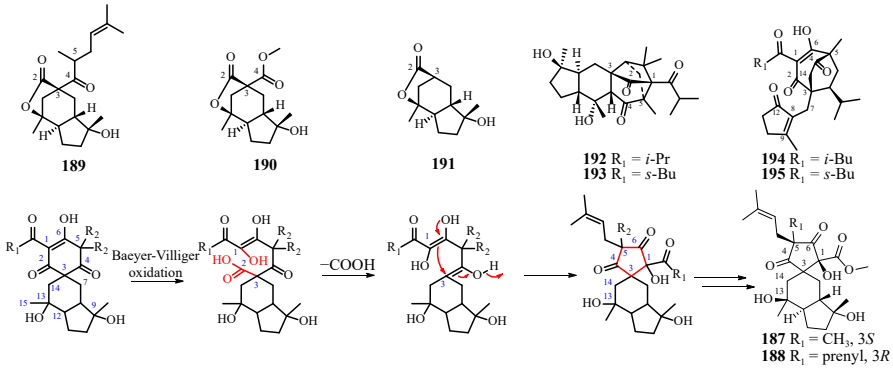

Fig. 20 Structures of **189**–**195**, and possible biosynthetic pathways of **187** and **188**.

two 6-*nor*-complicated PPAPs with an unprecedented tetracyclic system, hyperinoids A (**199**) and B (**200**) [118]. These compounds were proposed to biogenetically originate from an MPAP precursor through key intramolecular cyclization, oxidative cleavage of the C-5/C-6 bond, decarboxylation, and cyclization (Fig. 21). The structure of **199** was further confirmed by X-ray crystallographic data.

3. Biological activities

Seco- and *nor*-PPAPs, with their novel structural skeletons, have garnered significant attention due to their potent biological activities. These activities encompass anti-cancer, anti-inflammatory, hepatoprotective, anti-AD, MDR reversal, anti-depressant, neuroprotective, and immunosuppressive effects (Fig. 22). Among the reported compounds, twenty-nine *seco*- and *nor*-PPAPs demonstrated anti-cancer and MDR reversal activities. Additionally, 14 and 9 *seco*- and *nor*-PPAPs exhibited notable anti-AD and anti-depressant activities, respectively. Specifically, 10 *nor*-PPAPs showed potent anti-AD effects, while 6 displayed significant anti-depressant properties. This section provides a comprehensive summary and discussion of the diverse biological activities of *seco*- and *nor*-PPAPs (Tables S8–S16).

3.1. Anti-cancer activity

Approximately one-third of the compounds among 200 *seco*- and *nor*-PPAPs exhibited cytotoxic activity against various human cancer cell lines (Table S8). Several of these compounds demonstrated potent anti-cancer activity [half maximal inhibitory concentration (IC_{50}) < 10 μmol·L^{-1}], suggesting their potential as promising antitumor agents. Consequently, anti-cancer activity stands out as a notable characteristic of these PPAPs.

Hyperuralone E (**9**) and hyperfol A (**19**) exhibited activity against leukemia cell lines HEL and K562 with IC_{50} values ranging from 5.01 to 8.69 μmol·L^{-1}. These compounds induced apoptosis in HEL cells in a dose-dependent manner, with **9** increasing the expression of two marker proteins of apoptosis and cleavage of caspase-3 and PARP1 [39]. Thoreliolide B (**33**) demonstrated moderate cytotoxic activities against MCF-7, HeLa, and NCI-H460 tumor cell lines with IC_{50} values of 9.7, 16.6, and 24.2 μmol·L^{-1}, respectively [47]. Hunascynols A (**75**) (IC_{50} 6.87 μmol·L^{-1}) and B (**76**) (IC_{50} 9.86 μmol·L^{-1}) showed potent anti-proliferative effects against HCT116, surpassing the positive control 5-FU (IC_{50} 22.12 μmol·L^{-1}). These compounds induced G_1 phase arrest and inhibited the expression of STAT3, Smad4, and Snail [70]. Hyperbeanone A (**80**) exhibited remarkable cytotoxic activities by inducing G_1 phase cell cycle arrest and apoptosis in HL-60 and SU-DHL-4 cell lines with IC_{50} values of 7.07 and 12.49 μmol·L^{-1}, respectively [74]. Norhyperpalum B (**99**) showed good activity against hepatoma cell lines Hep3B, HepG2, SMMC-7721, and Huh-7 with IC_{50} values ranging from 9.48 to 18.67 μmol·L^{-1}, while norhyperpalums C–E (**100**, **98**, and **97**) demonstrated weak activities. The structural comparison suggested that the benzene group and stereochemistry at the 1,6-dioxaspiro[4.4]nonane moiety might play crucial roles in cytotoxicity [24]. Norascyronone A (**130**) exhibited cytotoxicity against SK-BR-3 (IC_{50} 4.3 μmol·L^{-1}) and PANC-1 (IC_{50} 8.4 μmol·L^{-1}) cell lines, while norascyronone B (**131**) showed a selective cytotoxic effect against SK-BR-3 (IC_{50} 7.8 μmol·L^{-1}) cell lines [23]. Additionally, hyperhexanone D (**135**) demonstrated mild anti-proliferative effects against HL-60 and NB4 cells with IC_{50} values ranging from 8.1 to 11.7 μmol·L^{-1} [92]. Yezo'otogirin C (**140**) displayed potential cytotoxic effects against MGc80-3 with an IC_{50} value of 9.54 μmol·L^{-1} [101], and spihyperglucinol A (**194**) exhibited satisfactory cytotoxicity against HL60 with an IC_{50} value of 9.12 μmol·L^{-1} [65].

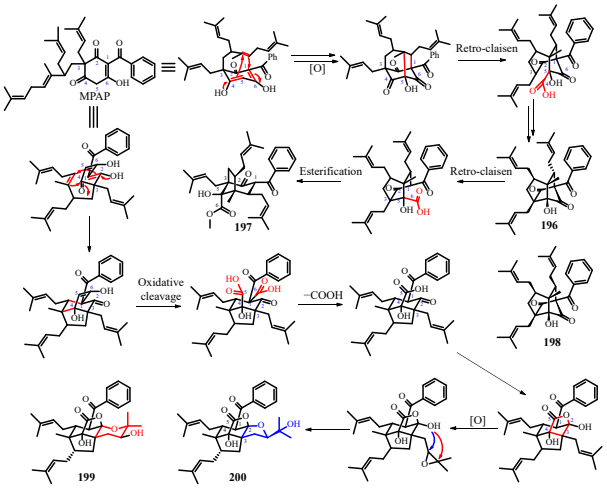

Fig. 21 Possible biosynthetic pathways of **196**–**200**.

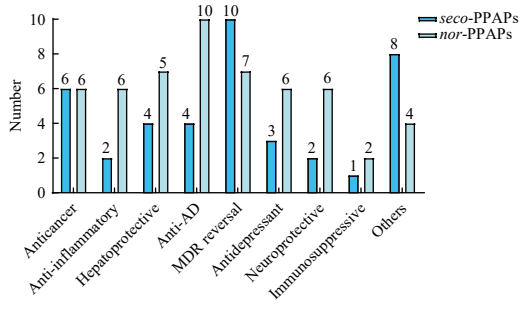

Fig. 22 Overview of potent biological activities of *seco*- and *nor*-PPAPs.

3.2. Anti-inflammatory activity

The majority of *Hypericum* species are utilized in traditional medicine for treating inflammatory conditions, including wounds, bruises, hepatitis, and acute mastitis, suggesting that their secondary metabolites possess significant anti-inflammatory properties [3, 119, 120]. A diverse range of structurally distinct *seco*- and *nor*-PPAPs have demonstrated anti-inflammatory activities by inhibiting the production of anti-inflammatory factors or inflammatory-related enzymes (Table S9).

Hypatulone A (**58**) demonstrated moderate NO inhibitory activity in an LPS-stimulated RAW264.7 cell model with an IC_{50} value of 18.8 ± 1.75 μmol·L^{-1}, surpassing *N*-monomethyl-L-arginine (IC_{50} 39.2 ± 0.36 μmol·L^{-1}, a positive control) [61, 62]. Longisglucinol A (**86**) and spihyperglucinols A (**194**) and B (**195**) inhibited LPS-induced NO production with IC_{50} values of 9.46 ± 1.21, 8.70 ± 1.18, and 9.23 ± 1.26 μmol·L^{-1}, respectively [65, 77]. **86** suppressed proinflammatory factors nuclear factor κB (NF-κB), interleukin-6 (IL-6), IL-1β, TGF-β1, and enhanced anti-inflammatory factors ARG1 and cluster of differentiation 206 (CD206) expression at the messenger ribonucleic acid (mRNA) level, suggesting its potential as an anti-inflammatory agent [77]. Soniiglucinols A (**185**) and B (**186**) inhibited NO production in RAW264.7 cells with IC_{50} values of 4.23 and 7.58 μmol·L^{-1}, respectively, and COX-2 activities with IC_{50} values of 5.27 and 8.32 μmol·L^{-1}, respectively, a characteristic of chronic inflammation [112]. **185** decreased the production of various inflammatory factors in a dose-dependent manner, including PGE2, tumor necrosis factor α (TNF-α), and IL-1β, and significantly inhibited the LPS-induced nuclear translocation of NF-κB p65, supporting its anti-inflammatory and enzyme inhibitory properties [112]. Additionally, NF-κB pathway luciferase assays revealed that hyperinoids A (**199**) and B (**200**) exhibited significant inhibitory activities in HEK293/NF-κB cells stimulated with TNF-α with IC_{50} of 0.75 and 1.19 μmol·L^{-1}, respectively, compared to positive control bortezomib (IC_{50} 0.07 μmol·L^{-1}). Concurrently, **199** and **200** suppressed the mRNA levels of certain proinflammatory genes, including IL-1β, IL-6,

and iNOS in RAW246.7 macrophages and primary mouse BMDM cells, indicating significant anti-inflammatory potential [118].

3.3. Hepatoprotective activity

Seco- and *nor*-PPAPs demonstrated significant hepatoprotective properties (Table S10). Hyperascyrin N (**39**) [51], hyperacmosin R (**107**) [86], hyperibrin G (**126**) [121], hyperscabrone I (**149**) [68], and compound **161** [121] exhibited hepatoprotective activities at 10 μmol·L^{-1} against paracetamol-induced HepG2 cell damage, with bicyclol or glutathione serving as positive controls. Hyphenrone A (**4**) and hyperscabin K (**159**) demonstrated hepatoprotective effects at 10 μmol·L^{-1} against DGalN-induced WB-F344 cell damage, with cell viabilities of 73% and 77%, respectively [32]. Hyperacmosins C (**28**) and D (**29**), as well as hyperacmosin E (**184**), exhibited potent hepatoprotective activity against paracetamol-induced HepG2 cell damage, showing cell viabilities of 56.31%, 55.10%, and 58.17%, respectively, compared to the hepatoprotective drug bicyclol as a positive control [45, 114]. The structural comparison suggested that the *s*-butyl at C-10 might enhance hepatoprotective activity. Hypericumoxide N (**105**) displayed moderate hepatoprotective activity in the D-galactosamine-induced HL-7702 cell model [84].

3.4. Anti-AD activity

AD is a complex neurodegenerative disorder. Cholinesterase (ChE), including AChE and BChE, collectively regulate neurotransmitter levels, while protein phosphatase-2A (PP2A) and protein cleaving enzyme 1 (BACE1) influence *β*-amyloid (A*β*) production, representing significant biological targets in AD [122-124]. To date, nineteen *seco*- and *nor*-PPAPs have been evaluated for anti-AD activity (Table S11). Hyperuralones C (**7**) and D (**8**) demonstrated moderate AChE inhibitory activities with IC_{50} values of 9.6 and 7.1 μmol·L^{-1}, respectively, compared to tacrine as a positive control (IC_{50} 0.33 μmol·L^{-1}) [37]. Two novel *seco*-PPAPs, hybeanones A (**73**) and B (**74**), exhibited potential AChE inhibitory potencies, with **74** showing superior binding affinity to **73** in molecular docking analysis [69]. Hyperforones F–H (**110**–**112**), A–E (**163**–**167**), I (**168**) and J (**170**) enhanced PP2A activity with EC_{50} values ranging from 199.0–7761.0 nmol·L^{-1}, and inhibited BACE1 activity with IC_{50} values ranging from 98.6–9553.0 nmol·L^{-1}. Notably, **110** and **166** demonstrated remarkable PP2A activation with EC_{50} values of 199.0 and 258.8 nmol·L^{-1}, respectively, and BACE1 inhibition with IC_{50} values of 98.6 and 136.2 nmol·L^{-1}, respectively, surpassing the positive controls SCR1693 and LY2811376. Molecular docking analysis of **110** and **111** indicated the propan-2-ol group's significant role in PP2A and BACE1 interactions. **110** demonstrated superior efficacy in alleviating pathological and cognitive impairment in 3 × Tg AD mice compared to LY2811376, positioning it as a promising lead compound for AD treatment [89].

3.5. MDR reversal activity

Seco- and *nor*-PPAPs from the genus *Hypericum* demonstrate potential multidrug reversal activities against adriamycin (ADR) resistant cancer cell lines, such as HepG2/ADR and MCF-7/ADR (Table S12). Hyperhexanone F (**24**) was identified as a potential modulator of MDR in MCF-7/ADR cells, exhibiting a higher reversal fold (RF = 38) than the positive control (verapamil, RF = 20) at the same concentration of 10 μmol·L^{-1} [33]. Four *seco*-PPAPs, biyoulactones A (**64**) and B (**65**) [66, 67], and hypemoins A (**67**) and B (**68**) [67], exhibited moderate reversal activities against MCF-7/ADR cells at a concentration of 20 μmol·L^{-1}, with RFs ranging from 11 to 27. Hypermonones A–D (**69**–**72**), I (**146**), and H (**147**) displayed MDR reversal activities against MCF-7/ADR cells with RFs ranging from 11 to 153 at 20 μmol·L^{-1}. **146** demonstrated higher activity than the positive control (verapamil, RF = 53) [68]. Hypermogins B (**142**) and C (**143**), **146**, and **147** exhibited effective reversal activities for HepG2/ADR cells. Notably, **146** displayed a stronger reversal effect than verapamil (RF = 124) [68, 98].

3.6. Anti-depressant activity

H. perforatum has been traditionally utilized for treating mild to moderate depression [21, 22, 125]. Consequently, numerous pharmacological studies have examined the anti-depressant effects of secondary metabolites from the genera *Garcinia* and *Hypericum*. Hyperscabins D (**2**), J–L (**158**–**160**), hyphenrone A (**4**), and hyperuralone C (**7**) were assessed *in vitro* for their anti-depressant effects *via* the inhibition of ([^{3}H]-5-HT) and noradrenaline ([^{3}H]-NE) reuptake in rat brain synaptosomes, utilizing duluxetine as a positive control. The results indicated that these compounds exhibited significant inhibitory activities at 1 μmol·L^{-1} against [^{3}H]-NE [32]. Hyperscabins A (**94**) and B (**95**) demonstrated effective reuptake inhibition of [^{3}H]-5-HT [126]. Additionally, hypericumoxide N (**105**) displayed moderate activity against the [^{3}H]-5-HT mode (Table S13) [84].

3.7. Neuroprotective activity

Recent studies have revealed that certain *seco*- and *nor*-PPAPs exhibit significant neuroprotective properties. Hyphenrone A (**4**), compounds **128** and **151**, hyphenrone F (**171**), and hyperforen A (**173**) demonstrated moderate neuroprotective effects in corticosterone-induced PC12 cells (Table S14) [108]. Hypermonin A (**175**) showed superior protection of PC12 cells against corticosterone-induced injury compared to hypermonin B (**176**), suggesting that hydroxyl orientation influences neuroprotective activity [110]. Furthermore, hyperascyrin N (**39**) and hyperibrin A (**145**) exhibited protective effects on SK-N-SH cells against glutamate-induced damage [51, 104]. Hyperscabin A (**94**) enhanced cell viability in oxygen-glucose deprivation-induced damage in SH-SY5Y cells at a concentration of 10 μmol·L^{-1}. Notably, **94** demonstrated more potent activity than the positive control drug potassium-(1-hydroxypentyl)-benzoate (47.4%) [126].

3.8. Immunosuppressive activity

Several *seco*- and *nor*-PPAPs have demonstrated immunosuppressive properties (Table S15). Hypersonin A (**53**) and norwilsonnol A (**137**) inhibited the proliferation of murine splenocytes induced by anti-CD3/anti-CD28 monoclonal antibodies [59, 88]. Additionally, **137** exhibited inhibitory activity in anti-CD3/anti-CD30 mAb-induced human peripheral blood mononuclear cells with an IC_{50} of 8.21 ± 0.98 μmol·L^{-1}, suppressing the production of cytokines such as IFN-γ, TNF-α, IL-4, and IL-10 in both models. Hypaluton A (**178**) displayed moderate inhibitory activity with an IC_{50} of 6.86 ± 0.72 μmol·L^{-1} in LPS-induced murine B cells [25].

3.9. Others

In addition to the aforementioned activities, *seco*- and *nor*-PPAPs exhibited other notable properties (Table S16). Oblongifolin M (**38**) demonstrated more potent anti-EV71 activity with an IC_{50} of 16.1 ± 0.5 μmol·L^{-1}, surpassing the positive control, ribavirin (IC_{50} 253.1 ± 13.0 μmol·L^{-1}). Compound **40** displayed antiprotozoal activity, inhibiting the proliferation of *Trypanosoma brucei rhodesiense* and *Plasmodium falciparum*, with IC_{50} values of 3.07 ± 0.77 and 2.25 ± 0.10 μmol·L^{-1}, respectively. Hyperilongenol B (**84**) and hypatulin A (**196**) exhibited significant anti-bacterial activity against *Staphylococcus aureus* and *Bacillus subtilis*, respectively [76, 116].

The anti-coagulant activity of hymoin C (**59**) demonstrated its ability to inhibit rabbit platelet aggregation induced by the platelet-activating factor, with an IC_{50} value of 119.23 ± 11.85 μmol·L^{-1} [63]. Hyperbenzone A (**30**) exhibited dose-dependent anti-

lipid accumulation effects in a palmitic acid-induced HepG2 cell model [46], while hypersampone A (**114**) reduced lipid accumulation in an oleic acid-treated HepG2 cell model by suppressing FAS and ACACA protein expression [91]. Garcibractinols G (**44**) and H (**45**) displayed antihyperglycemic activity by enhancing glucose consumption in HepG2 cells, with **44** showing greater efficacy than the positive control, metformin [55]. Hypsampsonione A (**34**) exhibited moderate *α*-glucosidase inhibitory activity [48]. Norsampsone C (**91**) and norsampsone E (**183**) demonstrated potent, dose-dependent RXRa transcriptional inhibitory activities [26, 113].

4. Conclusions

This review comprehensively examines the occurrence, structural characteristics, potential biosynthetic pathways, and biological activities of naturally occurring *seco*- and *nor*-PPAPs. From January 1988 to June 2023, 88 *seco*-PPAPs and 112 *nor*-PPAPs with diverse skeletons have been documented, categorized into six groups. As distinctive subsets of PPAPs, *seco*- and *nor*-PPAPs exhibit novel oxygen or carbon rings, serving as crucial sources of structural diversity. Their significant structural variations stem from the degrees and locations of cleavage, ring formation, and substituent variety. Additionally, the presence of various double bonds or conjugated fragments enhances cyclization and rearrangement possibilities. Future discoveries of more *seco*- and *nor*-PPAPs are anticipated. These compounds' rearranged polycyclic systems typically feature multiple chiral centers and quaternary carbons, while polyisopentenyl groups increase molecular flexibility, complicating single crystal formation and thus structural determination, particularly stereochemistry. Given the structural revisions of some novel non-crystalline compounds, the proposed biosynthetic pathways of *seco*- and *nor*-PPAPs with new skeletons offer a valid approach to understanding and elucidating their structural features. This approach can be complemented by quantum chemical calculations such as DP4+, J-DP4+, and ANN to further confirm complex structures with multiple chiral centers, especially for non-crystalline compounds [62, 127, 128]. Chemical and biomimetic synthesis also provide effective methods for determining and validating structures assigned *via* NMR data [105, 129].

As previously mentioned, *seco*- and *nor*-PPAPs have garnered significant attention due to their diverse structures and intriguing biological activities. Research has primarily focused on their anti-cancer, anti-inflammatory, hepatoprotective, anti-AD, MDR reversal, anti-depressant, neuroprotective, and immunosuppressive properties. However, most studies have been limited to activity screening, with few exploring mechanisms and structure-activity relationships (SARs) analysis, largely due to the scarcity of available compounds. Consequently, the synthesis or modification of active *seco*- and *nor*-PPAPs could be crucial for a more comprehensive investigation of their bioactivities, presenting a valuable direction for future research. Concurrently, the majority of *seco*- and *nor*-PPAPs are derived from the Clusiaceae family, particularly the genus *Hypericum*, yet current studies have examined only a fraction of these plants. It has been reported that merely 10% of the 500 *Hypericum* species have been investigated [3]. Thus, the vast number of unexplored *Hypericum* species may serve as a promising resource pool for chemically diverse *seco*- and *nor*-PPAPs.

This review aims to offer a comprehensive overview of the structures, biosynthesis pathways, and bioactivities of *seco*- and *nor*-PPAPs. It will serve as a structural reference for future lead compounds and provide a theoretical foundation for exploring the medicinal potential of ethnomedicines in subsequent research and development efforts.

Funding

This work was supported by the National Natural Science Foundation for Distinguished Young Scholars (No. 81725021); the National Natural Science Foundation of China (Nos. 82003633, 32100321, and 32300335); the National Natural Science Foundation of Hubei Province (Nos. 2023AFB791 and 2023AFB530); and the Knowledge Innovation Project of Wuhan Science and Technology Bureau (No. 2023020201020534).

Supporting information

Additional information supporting this research can be obtained by contacting the corresponding authors *via* E-mail.

Declaration of competing interest

These authors have no conflict of interest to declare.

References

1 Yang XW, Grossman RB, Xu G. Research progress of polycyclic polyprenylated acylphloroglucinols. *Chem Rev*. 2018;118(7):3508-3558. https://doi.org/10.1021/acs.chemrev.7b00551.
2 Ciochina R, Grossman RB. Polycyclic polyprenylated acylphloroglucinols. *Chem Rev*. 2006;106(9):3963-3986. https://doi.org/10.1021/cr0500582.
3 Bridi H, Meirelles GC, von Poser GL. Structural diversity and biological activities of phloroglucinol derivatives from *Hypericum* species. *Phytochemistry*. 2018;155:203-232. https://doi.org/10.1016/j.phytochem.2018.08.002.
4 Marrelli M, Statti G, Conforti F. *Hypericum* spp.: an update on the biological activities and metabolic profiles. *Mini Rev Med Chem*. 2020;20(1):66-87. https://doi.org/10.2174/1389557519666190926120211.
5 Guttroff C, Baykal A, Wang H, et al. Polycyclic polyprenylated acylphloroglucinols: an emerging class of non-peptide-based MRSA- and VRE-active antibiotics. *Angew Chem Int Ed*. 2017;56(50):15852-15856. https://doi.org/10.1002/anie.201707069.
6 Phang Y, Wang X, Lu Y, et al. Bicyclic polyprenylated acylphloroglucinols and their derivatives: structural modification, structure-activity relationship, biological activity and mechanism of action. *Eur J Med Chem*. 2020;205:112646. https://doi.org/10.1016/j.ejmech.2020.112646.
7 Zur Bonsen AB, Peralta RA, Fallon T, et al. Intramolecular tricarbonyl-ene reactions and *α*-hydroxy-*β*-diketone rearrangements inspired by the biosynthesis of polycyclic polyprenylated acylphloroglucinols. *Angew Chem Int Ed*. 2022;61(34):e202203311. https://doi.org/10.1002/anie.202203311.
8 Phang YL, Liu S, Zheng C, et al. Recent advances in the synthesis of natural products containing the phloroglucinol motif. *Nat Prod Rep*. 2022;39(9):1766-1802. https://doi.org/10.1039/D1NP00077B.
9 Wen S, Boyce JH, Kandappa SK, et al. Regiodivergent photocyclization of dearomatized acylphloroglucinols: asymmetric syntheses of (−)-nemorosone and (−)-6-*epi*-garcimultiflorone A. *J Am Chem Soc*. 2019;141(28):11315-11321. https://doi.org/10.1021/jacs.9b05600.
10 Grenning AJ, Boyce JH, Porco JA. Rapid synthesis of polyprenylated acylphloroglucinol analogs *via* dearomative conjunctive allylic annulation. *J Am Chem Soc*. 2014;136(33):11799-11804. https://doi.org/10.1021/ja5060302.
11 Li S, Chen Q, Xie X, et al. Pd-catalyzed enantioselective dearomative allylic annulation to access PPAPs analogues. *Org Lett*. 2021;23(20):7824-7828. https://doi.org/10.1021/acs.orglett.1c02842.
12 George JH, Hesse MD, Baldwin JE, et al. Biomimetic synthesis of polycyclic polyprenylated acylphloroglucinol natural products isolated from *Hypericum papuanum*. *Org Lett*. 2010;12(15):3532-3535. https://doi.org/10.1021/ol101380a.
13 Wang X, Phang Y, Feng J, et al. Stereodivergent strategy in structural determination: asymmetric total synthesis of garcinol, cambogin, and related analogues. *Org Lett*. 2021;23(11):4203-4208. https://doi.org/10.1021/acs.orglett.1c01139.
14 Pepper HP, Tulip SJ, Nakano Y, et al. Biomimetic total synthesis of (±)-doitunggarcinone A and (+)-garcibracteatone. *J Org Chem*. 2014;79(6):2564-2573. https://doi.org/10.1021/jo500027k.
15 Simpkins NS. Adventures in bridgehead substitution chemistry: synthesis of polycyclic polyprenylated acylphloroglucinols (PPAPs). *Chem Commun*. 2013;49(11):1042-1051. https://doi.org/10.1039/C2CC37914G.
16 Ji Y, Hong B, Franzoni I, et al. Enantioselective total synthesis of hyperforin and pyrohyperforin. *Angew Chem Int Ed*. 2022;61(16):e202116136. https://doi.org/10.1002/anie.202116136.
17 Li XX, Yan Y, Zhang J, et al. Hyperforin: a natural lead compound with multiple pharmacological activities. *Phytochemistry*. 2023;206:113526. https://doi.org/10.1016/j.phytochem.2022.113526.
18 Liu S, Yu B, Dai J, et al. Targeting the biological activity and biosynthesis of hyperforin: a mini-review. *Chin J Nat Med*. 2022;20(10):721-728. https://doi.org/10.1016/S1875-5364(22)60189-4.
19 Bystrov NS, Chernov BK, Dobrynin VN, et al. The structure of hyperforin. *Tetrahedron Lett*. 1975;16(32):2791-2794. https://doi.org/10.1016/S0040-4039(00)75241-5.
20 Richard JA. Chemistry and biology of the polycyclic polyprenylated acylphloroglucinol hyperforin. *Eur J Org Chem*. 2013;2014(2):273-299. https://doi.org/10.1002/ejoc.201300815.
21 Cervo L, Rozio M, Ekalle-Soppo CB, et al. Role of hyperforin in the antidepressant-like activity of *Hypericum perforatum* extracts.

Psychopharmacology. 2002;164(4):423-428. https://doi.org/10.1007/s00213-002-1229-5.
22 Chatterjee SS, Nöldner M, Koch E, et al. Antidepressant activity of *Hypericum perforatum* and hyperforin: the neglected possibility. *Pharmacopsychiatry*. 1998;31(Suppl 1):7-15. https://doi.org/10.1055/s-2007-979340.
23 Hu YL, Hu K, Kong LM, et al. Norascyrononeses A and B, 2,3,4-*nor*-polycyclic polyprenylated acylphloroglucinols from *Hypericum ascyron*. *Org Lett*. 2019;21(4):1007-1010. https://doi.org/10.1021/acs.orglett.8b04022.
24 Duan YL, Deng YF, Bu PF, et al. Discovery of *nor*-bicyclic polyprenylated acylphloroglucinols possessing diverse architectures with anti-hepatoma activities from *Hypericum patulum*. *Bioorg Chem*. 2021;111:104902. https://doi.org/10.1016/j.bioorg.2021.104902.
25 Duan YL, Xie SS, Bu PF, et al. Hypaluton A, an immunosuppressive 3,4-*nor*-polycyclic polyprenylated acylphloroglucinol from *Hypericum patulum*. *J Org Chem*. 2021;86(9):6478-6485. https://doi.org/10.1021/acs.joc.1c00319.
26 Tian WJ, Yu Y, Yao XJ, et al. Norsampsones A–D, four new decarbonyl polycyclic polyprenylated acylphloroglucinols from *Hypericum sampsonii*. *Org Lett*. 2014;16(13):3448-3451. https://doi.org/10.1021/ol501333k.
27 Kobayashi J, Tanaka N. Prenylated acylphloroglucinols and meroterpenoids from *Hypericum* plants. *Heterocycles*. 2015;90(1):23-40. https://doi.org/10.3987/REV-14-SR(K)1.
28 Richard JA, Pouwer RH, Chen DY. The chemistry of the polycyclic polyprenylated acylphloroglucinols. *Angew Chem Int Ed*. 2012;51(19):4536-4561. https://doi.org/10.1002/anie.201103873.
29 de Almeida MF, Guedes MLS, Cruz FG. Lathrophytoic acids A and B: two novel polyprenylated phloroglucinol derivatives from *Kielmeyera lathrophyton*. *Tetrahedron Lett*. 2011;52(52):7108-7112. https://doi.org/10.1016/j.tetlet.2011.10.102.
30 Cardona L, Pedro J, Serrano A, et al. Spiroterpenoids from *Hypericum Reflexum*. *Phytochemistry*. 1993;33(3):1185-1187. https://doi.org/10.1016/0031-9422(93)85046-T.
31 Fu YG, Huang YQ,Xu ZH, et al. Polyprenylated acylphloroglucinols from *Garcinia* species and structural revision of seven analogues. *Nat Prod Bioprospect*. 2025;15(1):34-47. https://doi.org/10.1007/s13659-025-00519-6.
32 Ma J, Zang YD, Zhang JJ, et al. Nine prenylated acylphloroglucinols with potential anti-depressive and hepatoprotective activities from *Hypericum scabrum*. *Bioorg Chem*. 2021;107:104529. https://doi.org/10.1016/j.bioorg.2020.104529.
33 Zhang ZZ, Zeng YR, Li YN, et al. Two new *seco*-polycyclic polyprenylated acylphloroglucinol from *Hypericum sampsonii*. *Org Biomol Chem*. 2021;19(1):216-219. https://doi.org/10.1039/D0OB02072A.
34 Yang XW, Ding Y, Zhang JJ, et al. New acylphloroglucinol derivatives with diverse architectures from *Hypericum henryi*. *Org Lett*. 2014;16(9):2434-2437. https://doi.org/10.1021/ol500808p.
35 Yang XW, Li MM, Liu X, et al. Polycyclic polyprenylated acylphloroglucinol congeners possessing diverse structures from *Hypericum henryi*. *J Nat Prod*. 2015;78(4):885-895. https://doi.org/10.1021/acs.jnatprod.5b00057.
36 Wu J, Cheng XF, Harrison LJ, et al. A phloroglucinol derivative with a new carbon skeleton from *Hypericum perforatum* (Guttiferae). *Tetrahedron Lett*. 2004;45(52):9657-9659. https://doi.org/10.1016/j.tetlet.2004.11.007.
37 Zhang JJ, Yang XW, Liu X, et al. 1,9-*Seco*-bicyclic polyprenylated acylphloroglucinols from *Hypericum uralum*. *J Nat Prod*. 2015;78(12):3075-3079. https://doi.org/10.1021/acs.jnatprod.5b00830.
38 Zhou ZB, Zhang YM, Pan K, et al. Cytotoxic polycyclic polyprenylated acylphloroglucinols from *Hypericum attenuatum*. *Fitoterapia*. 2014;95:1-7. https://doi.org/10.1016/j.fitote.2014.02.011.
39 Lou HY, Li YN, Yi P, et al. Hyperfols A and B: two highly modified polycyclic polyprenylated acylphloroglucinols from *Hypericum perforatum*. *Org Lett*. 2020;22(17):6903-6906. https://doi.org/10.1021/acs.orglett.0c02434.
40 Kong LM, Long XW, Yang XW, et al. *seco*-Polycyclic polyprenylated acylphloroglucinols with unusual carbon skeletons from *Hypericum ascyron*. *Tetrahedron Lett*. 2017;58(22):2113-2117. https://doi.org/10.1016/j.tetlet.2017.04.044.
41 Lu WJ, Xu WJ, Zhang MH, et al. Diverse polycyclic polyprenylated acylphloroglucinol congeners with anti-nonalcoholic steatohepatitis activity from *Hypericum forrestii*. *J Nat Prod*. 2021;84(4):1135-1148. https://doi.org/10.1021/acs.jnatprod.0c01202.
42 Verotta L, Lovaglio E, Sterner O, et al. Modulation of chemoselectivity by protein additives. Remarkable effects in the oxidation of hyperforin. *J Org Chem*. 2004;69(23):7869-7874. https://doi.org/10.1021/jo048857s.
43 Zhu H, Chen C, Yang J, et al. Hyperhexanone A, a crucial intermediate from bicyclo[3.3.1]- to cyclohexanone monocyclic-polycyclic polyprenylated acylphloroglucinols. *Tetrahedron*. 2016;72(31):4655-4659. https://doi.org/10.1016/j.tet.2016.06.035.
44 Sun M, Wang X, Zhu T, et al. Hyperacmosins K–M, three new polycyclic polyprenylated acylphloroglucinols from *Hypericum acmosepalum*. *RSC Adv*. 2021;11(34):21029-21035. https://doi.org/10.1039/D1RA03533A.
45 Suo XY, Shi MJ, Dang J, et al. Two new polycyclic polyprenylated acylphloroglucinols derivatives from *Hypericum acmosepalum*. *J Asian Nat Prod Res*. 2021;23(11):1068-1076. https://doi.org/10.1080/10286020.2021.1880395.
46 Lu W, Zhang Y, Li Y, et al. Hyperbenzones A and B, two 1,2-*seco* and rearranged polycyclic polyprenylated acylphloroglucinols from *Hypericum beanii*. *Chin Chem Lett*. 2022;33(8):4121-4125. https://doi.org/10.1016/j.cclet.2021.11.011.
47 Nguyen LTT, Lai NTDDT, Nguyen LTT, et al. Thoreliolides A and B, two polyisoprenylated benzoylphloroglucinol derivatives with a new carbon skeleton from the fruits of *Calophyllum thorelii*. *Tetrahedron Lett*. 2016;57(25):2737-2741. https://doi.org/10.1016/j.tetlet.2016.05.021.
48 Tao L, Xu S, Zhang Z, et al. Bioassay-guided isolation of *α*-glucosidase inhibitory constituents from *Hypericum sampsonii*. *Chin J Nat Med*. 2023;21(6):443-453. https://doi.org/10.1016/S1875-5364(23)60472-8.
49 Gao XM, Yu T, Lai FSF, et al. Novel polyisoprenylated benzophenone derivatives from *Garcinia paucinervis*. *Tetrahedron Lett*. 2010;51:2442-2446. https://doi.org/10.1016/j.tetlet.2010.02.147.
50 Zhang H, Tao L, Fu WW, et al. Prenylated benzoylphloroglucinols and xanthones from the leaves of *Garcinia oblongifolia* with antienteroviral activity. *J Nat Prod*. 2014;77(4):1037-1046. https://doi.org/10.1021/np500124e.
51 Zhen B, Hu JW, Wang JJ, et al. Hyperascyrins L–N, rare methylated polycyclic polyprenylated acylphloroglucinol derivatives from *Hypericum ascyron*. *J Asian Nat Prod Res*. 2019;21(5):409-418. https://doi.org/10.1080/10286020.2019.1581175.
52 Soroury S, Alilou M, Gelbrich T, et al. Unusual derivatives from *Hypericum scabrum*. *Sci Rep*. 2021;10(1):22181-22190. https://doi.org/10.1038/s41598-020-79305-y.
53 Andreas B, Christopher JS, Jonathan HG. Bioinspired total synthesis of hyperireflexolides A and B. *Org Lett*. 2023;25:6317-6321. https://doi.org/10.1021/acs.orglett.3c02232.
54 Winkelmann K, Heilmann J, Zerbe O, et al. Further prenylated bi- and tricyclic phloroglucinol derivatives from *Hypericum papuanum*. *Helv Chim Acta*. 2001;84(11):3380-3392. https://doi.org/10.1002/1522-2675(20011114)84:11<3380::AID-HLCA3380>3.0.CO;2-O.
55 Li X, Li Q, Xu J, et al. Isolation and antihyperglycemic effects of garcibractinols A–H, intricate polycyclic polyprenylated acylphloroglucinols from the fruits of *Garcinia bracteata*. *Bioorg Chem*. 2023;138:106651. https://doi.org/10.1016/j.bioorg.2023.106651.
56 Lu WJ, Xu WJ, Zhang YQ, et al. Hyperforones A–C, benzoyl-migrated [5.3.1]-type polycyclic polyprenylated acylphloroglucinols from *Hypericum forrestii*. *Org Chem Front*. 2020;7(9):1070-1076. https://doi.org/10.1039/D0QO00152J.
57 Liao Y, Liu X, Yang J, et al. Hypersubones A and B, new polycyclic acylphloroglucinols with intriguing adamantane type cores from *Hypericum subsessile*. *Org Lett*. 2015;17(5):1172-1175. https://doi.org/10.1021/acs.orglett.5b00100.
58 Ye Y, Yang XW, Xu G. Unusual adamantane type polyprenylated acylphloroglucinols with an oxirane unit and their structural transformation from *Hypericum hookerianum*. *Tetrahedron*. 2016;72(22):3057-3062. https://doi.org/10.1016/j.tet.2016.04.025.
59 Xie S, Tan X, Liu Y, et al. Hypersonins A–D, Polycyclic polyprenylated acylphloroglucinols with a 1,2-*seco*-homoadamantane architecture from *Hypericum wilsonii*. *J Nat Prod*. 2020;83(6):1804-1809. https://doi.org/10.1021/acs.jnatprod.9b01187.
60 Teng H, Ren Y, Ma Z, et al. Homoadamantane polycyclic polyprenylated acylphloroglucinols from the fruits of *Garcinia multiflora*. *Fitoterapia*. 2019;137:104245. https://doi.org/10.1016/j.fitote.2019.104245.
61 Liu YY, Ao Z, Xue GM, et al. Hypatulone A, a homoadamantane-type acylphloroglucinol with an intricately caged core from *Hypericum patulum*. *Org Lett*. 2018;20(24):7953-7956. https://doi.org/10.1021/acs.orglett.8b03523.
62 Yang XW, Grossman RB. Revision of the structure of hypatulone A by NMR, computations, and biosynthetic considerations. *Org Lett*. 2020;22(2):760-763. https://doi.org/10.1021/acs.orglett.9b04666.
63 Zeng YR, Yuan CM, Li YN, et al. Hymoins A–D: two pairs of polyprenylated acylphloroglucinols from *Hypericum monogynum* and their light-induced transformation. *Org Lett*. 2021;23(8):3125-3129. https://doi.org/10.1021/acs.orglett.1c00811.
64 Li YW, Lu WJ, Zhou X, et al. Diverse polycyclic polyprenylated acylphloroglucinols with anti-neuroinflammatory activity from *Hypericum beanii*. *Bioorg Chem*. 2022;127:106005. https://doi.org/10.1016/j.bioorg.2022.106005.
65 Shi Z, Hu H, Guo Y, et al. Discovery of 13,15-*nor*-polycyclic polyprenylated acylphloroglucinols from *Hypericum longistylum* with anti-inflammatory activity. *Org Biomol Chem*. 2022;20(6):1284-1291. https://doi.org/10.1039/D1OB02107A.
66 Tanaka N, Abe S, Hasegawa K, et al. Biyoulactones A–C, new pentacyclic meroterpenoids from *Hypericum chinense*. *Org Lett*. 2011;13(20):5488-5491. https://doi.org/10.1021/ol2021548.
67 Li YN, Zeng YR, Yang J, et al. Chemical constituents from the flowers of *Hypericum monogynum* L. with COX-2 inhibitory activity. *Phytochemistry*. 2022;193:112970. https://doi.org/10.1016/j.phytochem.2021.112970.
68 Zeng YR, Li YN, Yang J, et al. Hypermonones A–I, new polyprenylated acylphloroglucinols from *Hypericum monogynum* with multidrug resistance reversal activity. *Chin J Chem*. 2021;39(9):2422-2432. https://doi.org/10.1002/cjoc.202100210.
69 Yang B, Qi C, Yao Z, et al. Hybeanones A and B, two highly modified polycyclic polyprenylated acylphloroglucinols from *Hypericum beanii*. *Chin J Chem*. 2022;40(1):53-58. https://doi.org/10.1002/cjoc.202100468.
70 Hu YL, Yue GG, Li XR, et al. Structurally diverse spirocyclic polycyclic polyprenylated acylphloroglucinols from *Hypericum ascyron* Linn. and their anti-tumor activity. *Phytochemistry*. 2023;212:113727. https://doi.org/10.1016/j.phytochem.2023.113727.
71 Xu WJ, Luo J, Li RJ, et al. Furanmonogones A and B: two rearranged acylphloroglucinols with a 4,5-*seco*-3(2*H*)-furanone core from the flowers of *Hypericum monogynum*. *Org Chem Front*. 2017;4(2):313-317. https://doi.org/10.1039/C6QO00620E.
72 Li D, Yang J, Liu B, et al. Synthesis of desacyl furanmonogones A and B. *Org Lett*. 2021;23(12):4532-4537. https://doi.org/10.1021/acs.orglett.1c01157.
73 Duan YT, Zhang J, Lao YZ, et al. Spirocyclic polycyclic polyprenylated acylphloroglucinols from the ethyl acetate fraction of *Hypericum henryi*. *Tetrahedron Lett*. 2018;59(46):4067-4072. https://doi.org/10.1016/j.tetlet.2018.09.071.
74 Yang B, Huang J, Lin S, et al. Hyperbeanone A, a 5,6-*seco*-spirocyclic polycyclic polyprenylated acylphloroglucinol derivative with an unprecedented skeleton from *Hypericum beanii*. *Org Chem Front*. 2021;8(22):6411-6418. https://doi.org/10.1039/D1QO01302E.
75 Tanaka N, Abe S, Kobayashi Ji. Biyoulactones D and E, meroterpenoids from *Hypericum chinense*. *Tetrahedron Lett*. 2012;53(12):1507-1510. https://doi.org/10.1016/j.tetlet.2012.01.052.
76 Zhang N, Shi Z, Guo Y, et al. The absolute configurations of hyperilongenols A–C: rare 12,13-*seco*-spirocyclic polycyclic polyprenylated acylphloroglucinols with enolizable *β*,*β*′-tricarbonyl systems from *Hypericum longistylum* Oliv. *Org Chem Front*. 2019;6(9):1491-1502. https://doi.org/10.1039/C9QO00245F.
77 Zhang N, Shi Z, Xu Q, et al. Longisglucinols A–C, structurally intriguing polycyclic polyprenylated acylphloroglucinols with anti-inflammatory activity from *Hypericum longistylum*. *Org Lett*. 2020;22(20):7926-7929. https://doi.org/10.1021/acs.orglett.0c02853.
78 Chen Y, Xue Q, Teng H, et al. Acylphloroglucinol derivatives with a tricyclo-[4.4.1.1^{1,4}] dodecane skeleton from *Garcinia bracteata* fruits. *J Org Chem*.

2020;85(10):6620-6625. https://doi.org/10.1021/acs.joc.0c00637.
79 Tantapakul C, Phakhodee W, Ritthiwigrom T, et al. Rearranged benzophenones and prenylated xanthones from *Garcinia propinqua* twigs. *J Nat Prod*. 2012;75(9):1660-1664. https://doi.org/10.1021/np300487w.
80 Oya A, Tanaka N, Kusama T, et al. Prenylated benzophenones from *Triadenum japonicum*. *J Nat Prod*. 2015;78(2):258-264. https://doi.org/10.1021/np500827h.
81 Mitsugi K, Takabayashi T, Ohyoshi T, et al. Total synthesis of a PPAP, nemorosonol, using a tandem Michael addition-intramolecular aldol reaction. *Org Lett*. 2022;24(25):4635-4639. https://doi.org/10.1021/acs.orglett.2c01745.
82 Nigam SK, Banerji R, Rebuffat S, et al. Soulattrone A, a C_{24} terpenoid from *Calophyllum soulattri*. *Phytochemistry*. 1988;27(2):527-530. https://doi.org/10.1016/0031-9422(88)83134-0.
83 Zheng C, Wang X, Fu W, et al. Total synthesis of norsampsones A and B, garcinielliptones N and O, and hyperscabrin A. *J Nat Prod*. 2018;81(11):2582-2589. https://doi.org/10.1021/acs.jnatprod.8b00763.
84 Liu R, Su Y, Yang J, et al. Polyprenylated acylphloroglucinols from *Hypericum scabrum*. *Phytochemistry*. 2017;142:38-50. https://doi.org/10.1016/j.phytochem.2017.06.011.
85 Zhang F, Yang J, Yi P, et al. Hyperpatone A, a polycyclic polyprenylated acylphloroglucinol with a rare 8/6/5/6/5 pentacyclic skeleton from *Hypericum patulum*. *Org Biomol Chem*. 2023;21:140-146. https://doi.org/10.1039/D2OB01851A.
86 Ma Y, Liu B, Li P, et al. Hyperacmosin R, a new decarbonyl prenylphloroglucinol with unusual spiroketal subunit from *Hypericum acmosepalum*. *Molecules*. 2022;27:5932. https://doi.org/10.3390/molecules27185932.
87 Teng H, Ma Z, Teng H, et al. Two novel cyclohexanone-monocyclic polycyclic polyprenylated acylphloroglucinols from *Garcinia multiflora* fruits. *Nat Prod Res*. 2022;36(2):508-514. https://doi.org/10.1080/14786419.2020.1788559.
88 Xie S, Zhou Y, Tan X, et al. Norwilsonnol A, an immunosuppressive polycyclic polyprenylated acylphloroglucinol with a spiro[5-oxatricyclo [6.4.0.0^{3,7}]dodecane-6',1-1',2'-dioxane] system from *Hypericum wilsonii*. *Org Chem Front*. 2021;8(10):2280-2286. https://doi.org/10.1039/D1QO00271F.
89 Guo Y, Huang F, Sun W, et al. Unprecedented polycyclic polyprenylated acylphloroglucinols with anti-Alzheimer's activity from St. John's wort. *Chem Sci*. 2021;12(34):11438-11446. https://doi.org/10.1039/D1SC03356E.
90 Duan Y, Guo Y, Deng Y, et al. Norprzewalsone A, a rearranged polycyclic polyprenylated acylphloroglucinol with a spiro[cyclopentane-1,3'-tricyclo [7.4.0.0^{1,6}]tridecane] core from *Hypericum przewalskii*. *J Org Chem*. 2022;87(10):6824-6831. https://doi.org/10.1021/acs.joc.2c00503.
91 Huang L, Zhang Z, Li YN, et al. Hypersampones A–C, three *nor*-polycyclic polyprenylated acylphloroglucinols with lipid-lowering activity from *Hypericum sampsonii*. *Org Lett*. 2022;24:5967-5971. https://doi.org/10.1021/acs.orglett.2c02240.
92 Guo Y, Tong Q, Zhang N, et al. Highly functionalized cyclohexanone-monocyclic polyprenylated acylphloroglucinols from *Hypericum perforatum* induce leukemia cell apoptosis. *Org Chem Front*. 2019;6(6):817-824. https://doi.org/10.1039/C8QO01268G.
93 Sun H, Wang J, Zhen B, et al. Polycyclic polyprenylated acylphloroglucinol derivatives from *Hypericum pseudohenryi*. *Phytochemistry*. 2021;187:112761. https://doi.org/10.1016/j.phytochem.2021.112761.
94 Xu ZJ, Liu XY, Zhu MZ, et al. Photoredox-catalyzed cascade reactions involving aryl radical: total synthesis of (±)-norascyronone A and (±)-eudesmol. *Org Lett*. 2021;23(23):9073-9077. https://doi.org/10.1021/acs.orglett.1c03319.
95 Sassnink SA, Phan QD, Lam HC, et al. Biomimetic synthesis of the non-canonical PPAP natural products yezo'otogirin C and hypermogin D, and studies towards the synthesis of norascyronone A. *Org Biomol Chem*. 2022;20(8):1759-1768. https://doi.org/10.1039/D2OB00074A.
96 Cao T, Zhu L, Lan Y, et al. Protecting-group-free total syntheses of (±)-norascyronones A and B. *Org Lett*. 2020;22(7):2517-2521. https://doi.org/10.1021/acs.orglett.0c00212.
97 Tanaka N, Kakuguchi Y, Ishiyama H, et al. Yezo'otogirins A–C, new tricyclic terpenoids from *Hypericum yezoense*. *Tetrahedron Lett*. 2009;50(33):4747-4750. https://doi.org/10.1016/j.tetlet.2009.06.021.
98 Zeng Y, Yang J, Li Y, et al. Hypermogins A–D, four highly modified polycyclic polyprenylated acylphloroglucinols from *Hypericum monogynum*. *Tetrahedron Lett*. 2021;64:152733. https://doi.org/10.1016/j.tetlet.2020.152733.
99 Lam HC, Kuan KK, George JH. Biomimetic total synthesis of (±)-yezo'otogirin A. *Org Biomol Chem*. 2014;12(16):2519-2522. https://doi.org/10.1039/C4OB00186A.
100 He S, Yang W, Zhu L, et al. Bioinspired total synthesis of (±)-yezo'otogirin C. *Org Lett*. 2014;16(2):496-499. https://doi.org/10.1021/ol403374h.
101 Yang W, Cao J, Zhang M, et al. Systemic study on the biogenic pathways of yezo'otogirins: total synthesis and antitumor activities of (±)-yezo'otogirin C and its structural analogues. *J Org Chem*. 2015;80(2):836-846. https://doi.org/10.1021/jo502267g.
102 Shan MD, Hu LH, Chen ZL. Three new hyperforin analogues from *Hypericum perforatum*. *J Nat Prod*. 2001;64(1):127-130. https://doi.org/10.1021/np000362k.
103 Ma J, Ji TF, Yang JB, et al. Three new phloroglucinol derivatives from *Hypericum scabrum*. *J Asian Nat Prod Res*. 2012;14(5):508-514. https://doi.org/10.1080/10286020.2012.680445.
104 Gao W, Hu JW, Hou WZ, et al. Four new prenylated phloroglucinol derivatives from *Hypericum scabrum*. *Tetrahedron Lett*. 2016;57(21):2244-2248. https://doi.org/10.1016/j.tetlet.2016.04.026.
105 Wang X, Nie XB, Grossman RB, et al. Structural revision of hyperibrin B and hyperscabrones H and I by biosynthetic considerations, NMR analysis, and chemical synthesis. *J Nat Prod*. 2021;84(7):2059-2064. https://doi.org/10.1021/acs.jnatprod.1c00458.
106 Gao W, Hou WZ, Zhao J, et al. Polycyclic polyprenylated acylphloroglucinol congeners from *Hypericum scabrum*. *J Nat Prod*. 2016;79(6):1538-1547. https://doi.org/10.1021/acs.jnatprod.5b01063.
107 Weng JR, Tsao LT, Wang JP, et al. Anti-inflammatory phloroglucinols and terpenoids from *Garcinia subelliptica*. *J Nat Prod*. 2004;67(11):1796-1799. https://doi.org/10.1021/np049811x.
108 Lou H, Ma F, Yi P, et al. Bioassay and UPLC-Q-Orbitrap-MS/MS guided isolation of polycyclic polyprenylated acylphloroglucinols from St. John's wort and their neuroprotective activity. *Arab J Chem*. 2022;15:104057. https://doi.org/10.1016/j.arabjc.2022.104057.
109 Fang QQ, Feng TT, Wang AZ, et al. Structurally diverse polyprenylated acylphloroglucinols from *Hypericum uralum* Buch. Ham. ex D. Don. *Phytochemistry*. 2021;187:112771. https://doi.org/10.1016/j.phytochem.2021.112771.
110 Zeng YR, Yi P, Gu W, et al. Hypermonins A and B, two 6-norpolyprenylated acylphloroglucinols with unprecedented skeletons from *Hypericum monogynum*. *Org Biomol Chem*. 2018;16(22):4195-4198. https://doi.org/10.1039/C8OB00650D.
111 Zheng D, Chen Y, Wan S, et al. Polycyclic polyprenylated acylphloroglucinol congeners from *Garcinia yunnanensis* Hu with inhibitory effect on *α*-hemolysin production in *Staphylococcus aureus*. *Bioorg Chem*. 2021;114:105074. https://doi.org/10.1016/j.bioorg.2021.105074.
112 Xie S, Qi C, Duan Y, et al. Discovery of new polycyclic polyprenylated acylphloroglucinols with diverse architectures as potent cyclooxygenase-2 inhibitors. *Org Chem Front*. 2020;7(11):1349-1357. https://doi.org/10.1039/D0QO00259C.
113 Tian WJ, Qiu YQ, Chen JJ, et al. Norsampsone E, an unprecedented decarbonyl polycyclic polyprenylated acylphloroglucinol with a homoadamantyl core from *Hypericum sampsonii*. *RSC Adv*. 2017;7(53):33113-33119. https://doi.org/10.1039/C7RA05947G.
114 Wang X, Shi M, Wang J, et al. Hyperacmosins E–G, three new homoadamantane-type polyprenylated acylphloroglucinols from *Hypericum acmosepalum*. *Fitoterapia*. 2020;142:104535. https://doi.org/10.1016/j.fitote.2020.104535.
115 Tanaka N, Kashiwada Y, Kim SY, et al. Acylphloroglucinol, biyouyanagiol, biyouyanagin B, and related spiro-lactones from *Hypericum chinense*. *J Nat Prod*. 2009;72(8):1447-1452. https://doi.org/10.1021/np900109y.
116 Tanaka N, Yano Y, Tatano Y, et al. Hypatulins A and B, meroterpenes from *Hypericum patulum*. *Org Lett*. 2016;18(20):5360-5363. https://doi.org/10.1021/acs.orglett.6b02725.
117 Leisering S, Ponath S, Shakeri K, et al. Synthesis of 3-*epi*-hypatulin B featuring a late-stage photo-oxidation in flow. *Org Lett*. 2022;24(24):4305-4309. https://doi.org/10.1021/acs.orglett.2c00689.
118 Jia X, Wu Y, Lei C, et al. Hyperinoids A and B, two polycyclic meroterpenoids from *Hypericum patulum*. *Chin Chem Lett*. 2020;31(5):1263-1266. https://doi.org/10.1016/j.cclet.2019.10.014.
119 Zhang R, Ji Y, Zhang X, et al. Ethnopharmacology of *Hypericum* species in China: a comprehensive review on ethnobotany, phytochemistry and pharmacology. *J Ethnopharmacol*. 2020;254:112686. https://doi.org/10.1016/j.jep.2020.112686.
120 Zhang R, Ji Y, Morcol T, et al. UPLC-QTof-MS chemical profiling and characterization of antiproliferative and anti-inflammatory compounds from seven *Hypericum* species in China. *Ind Crop Prod*. 2021;173:114156. https://doi.org/10.1016/j.indcrop.2021.114156.
121 Hu J, Gao W, Xu F, et al. Polycyclic polyprenylated acylphloroglucinol derivatives from *Hypericum scabrum*. *Bioorg Med Chem Lett*. 2017;27(21):4932-4936. https://doi.org/10.1016/j.bmcl.2017.09.001.
122 Gong CX, Lidsky T, Wegiel J, et al. Phosphorylation of microtubule-associated protein Tau is regulated by protein phosphatase 2A in mammalian brain. Implications for neurofibrillary degeneration in Alzheimer's disease. *J Biol Chem*. 2000;275(8):5535-5544. https://doi.org/10.1074/jbc.275.8.5535.
123 Vassar R. Bace 1. *J Mol Neurosci*. 2004;23(1):105-113. https://doi.org/10.1385/JMN:23:1-2:105.
124 Tiwari S, Atluri V, Kaushik A, et al. Alzheimer's disease: pathogenesis, diagnostics, and therapeutics. *Int J Nanomed*. 2019;14:5541-5554. https://doi.org/10.2147/IJN.S200490.
125 Butterweck V. Mechanism of action of St John's wort in depression what is known ? *CNS Drugs*. 2003;17(8):539-562. https://doi.org/10.2165/00023210-200317080-00001.
126 Ma J, Xia G, Zang Y, et al. Three new decarbonyl prenylphloroglucinols bearing unusual spirost subunits from *Hypericum scabrum* and their neuronal activities. *Chin Chem Lett*. 2020;32:1173-1176. https://doi.org/10.1016/j.cclet.2020.07.037.
127 Tang Y, Xue Y, Du G, et al. Structural revisions of a class of natural products: scaffolds of aglycon analogues of fusicoccins and cotylenins isolated from fungi. *Angew Chem Int Ed*. 2016;55(12):4069-4073. https://doi.org/10.1002/anie.201600313.
128 Navarro-Vazquez A. Computational structural revision of a 4-hydroxy-3-(1'-angeloyloxy-2',3'-epoxy-3'-methyl)butylacetophenone compound from *Ageratina grandifolia*. *J Nat Prod*. 2021;84(7):2043-2047. https://doi.org/10.1021/acs.jnatprod.1c00398.
129 Grossman RB, Yang XW. Structural revision of garcinielliptin oxide and garcinielliptone E. *J Nat Prod*. 2020;83(6):2041-2044. https://doi.org/10.1021/acs.jnatprod.0c00306.